Title: TREM2 is downregulated by HSV1 in microglia and involved in antiviral defense in the brain

Authors: Stefanie Fruhwürth[1,2]*, Line S. Reinert[3], Carl Öberg[2†], Marcelina Sakr[2†], Marcus Henricsson[4], Henrik Zetterberg[2,5,6,7,8], Søren R. Paludan[1,3]*

Affiliations:

[1]Department of Rheumatology and Inflammatory Research, Institute of Medicine, Sahlgrenska Academy at the University of Gothenburg; Gothenburg, Sweden

[2]Department of Psychiatry and Neurochemistry, Institute of Neuroscience and Physiology, Sahlgrenska Academy at the University of Gothenburg; Gothenburg, Sweden

[3]Department of Biomedicine, Aarhus University; Aarhus, Denmark

[4]Biomarker Discovery and Development, Research and Early Development, Cardiovascular, Renal, and Metabolism (CVRM), BioPharmaceuticals R&D, AstraZeneca; Gothenburg, Sweden

[5]Clinical Neurochemistry Laboratory, Sahlgrenska University Hospital; Mölndal, Sweden

[6]Department of Neurodegenerative Disease, UCL Institute of Neurology; Queen Square, London, United Kingdom

[7]UK Dementia Research Institute at UCL; London, United Kingdom

[8]Hong Kong Center for Neurodegenerative Diseases; Clear Water Bay, Hong Kong, China

*Corresponding authors. Email: srp@biomed.au.dk, stefanie.fruhwurth@gu.se.

[†] These authors contributed equally to this work.

One Sentence Summary:
TREM2 is an important component of the antiviral immune response in microglia, which is actively targeted by HSV1.

Abstract:
Immunological control of viral infections in the brain exerts immediate protection, and also long-term maintenance of brain integrity. Microglia are important for antiviral defense in the brain. Here, we report that herpes simplex virus type 1 (HSV1) infection of human induced pluripotent stem cell (hiPSC)-derived microglia down-regulates expression of genes in the TREM2 pathway. TREM2 was found to be important for virus-induced *IFNB* induction through the DNA-sensing cGAS-STING pathway in microglia, and for phagocytosis of HSV1-infected neurons. Consequently, TREM2 depletion increased susceptibility to HSV1 infection in human microglia-neuron co-cultures and in the mouse brain. TREM2 augmented STING signaling and activation of down-stream targets TBK1 and IRF3. Thus, TREM2 is important for the antiviral immune response in microglia. Since *TREM2* loss-of-function mutations and HSV1 serological status are both linked to Alzheimer's disease, this work poses the question whether genetic or virus-induced alterations of TREM2 activity predisposes to post-infection neurological pathologies.

Main Text:

Introduction

Acute viral encephalitis is a severe disease, with often fatal outcome if untreated (*1*). Herpes simplex encephalitis (HSE) is the leading cause of viral encephalitis in the Western world and is caused by herpes simplex virus type 1 (HSV1) infection (*2, 3*). HSV1 is a neurotropic human DNA virus that can reach the central nervous system (CNS) via retrograde axon transport after infecting peripheral sensory neurons. Even though antiviral treatment is available for HSV1 and notably improves survival rates, post-HSE is often associated with serious sequelae. Between 50 and 80% of the adult population are HSV1-seropositive (*4*), and although HSE develops only in very few cases, epidemiological data have linked HSV1 infection with development of Alzheimer's disease (AD) (*5, 6*). Taken together, the available data therefore suggests that immunological control of HSV1 infection in the CNS is important for immediate protection of the brain and for long-term maintenance of brain integrity.

The early innate immune response is crucial to restrict HSV1 spread in the CNS. Microglia are the primary resident immune cells of the brain and protect the brain parenchyma against pathogen invasions through key macrophage functions, such as the release of antiviral type I interferons (IFN-I), cytokines, and phagocytosis of cell debris. Depletion of microglia increases viral spread in the CNS and consequently decreases the survival rates of mice infected with HSV1 (*7-9*). Optimal sensing and immune activation by microglia therefore require both continuous sampling of the local environment for danger signals, and pathogen sensing by a broad repertoire of innate pattern recognition receptors (PRRs).

For the sensing, microglia express high levels of numerous PRRs, including the cytosolic DNA sensor cyclic GMP-AMP synthase (cGAS). cGAS detects and binds to HSV1 DNA, leading to 2´3´cGAMP production and binding to stimulator of interferon genes (STING), which activates TANK-binding kinase 1 (TBK1) and interferon regulatory factor 3 (IRF3) (*10, 11*). Activated IRF3 translocates to the nucleus to activate the transcription of IFN-I genes, including *IFNB*. Consequently, numerous IFN-stimulated genes (ISGs) are induced to exert direct antiviral activity through interference with specific steps in the viral replication cycle. Additionally, cGAS induces expression of inflammatory cytokines, such as IL6 and TNFα, via the NFκB pathway. We previously reported that cGAS and STING are highly expressed in microglia, which utilize this pathway to produce the bulk of IFN-I in the HSV1-infected mouse brain (*12*). In humans, functional deficits in TBK1 or IRF3 are associated with HSE susceptibility (*13, 14*), and several viral mechanisms to antagonize STING signaling have been identified (*15-18*). Collectively, this suggests that the cGAS-STING signaling axis plays an important role in control of HSV1 infection in the CNS.

For the sampling of the brain during both homeostatic and pathological conditions, microglia use a panel of receptors that bind a broad range of charged and hydrophobic molecules. These include scavenger receptor A-1, CD36, receptor for advanced glycation end products (RAGE), and triggering receptor expressed on myeloid cells-2 (TREM2). TREM2 is primarily expressed by microglia and interacts with a wide range of ligands, including bacterial products, apoptotic cells, beta-amyloid (Aβ), anionic lipids, and apolipoprotein E (apoE) (*19*). Ligand engagement by TREM2 triggers downstream signaling through the adaptor protein DNAX activation protein 12 (DAP12) and recruitment and activation of the protein kinase SYK. In addition, TREM2 activity

can be regulated via proteolytic processing of the receptor which releases a soluble TREM2 fragment (sTREM2) (*20*), the function of which remains to be fully elucidated. In humans, loss-of-function mutations of *TREM2* or *DAP12* result in Nasu-Hakola disease, a serious disorder characterized by presenile dementia and bone cysts (*21, 22*). Gene variants causing reduced function of TREM2 increase the risk to develop AD several fold (*23, 24*). Less is known about the role of TREM2 during viral CNS infections. Studies investigating other neurotropic viruses, such as HHV-6A and HIV, suggest a link between altered TREM2 expression, inflammation, and neurocognitive disorders (*25, 26*). However, the role of TREM2 during CNS infection with HSV1 is unexplored.

The aim of this study was to explore how HSV1 modulates gene expression in human microglia and to determine the functional impact on control of HSV1 infection. Here, we report that HSV1 infection of human induced pluripotent stem cell (hiPSC)-derived microglia selectively down-regulates expression of genes in the TREM2 pathway. TREM2 was found to be important for viral activation of cGAS-STING signaling in microglia, and corresponding induction of the antiviral IFN-I response. Hence, TREM2 depletion in microglia and mice increased susceptibility to HSV1 infection both in human microglia-neuron co-cultures and *in vivo*, respectively. These data identify TREM2 as a component of the antiviral immune response in microglia, which is actively targeted by HSV1.

RESULTS

HSV1 selectively blocks transcripts of the TREM2 pathway in hiPSC-derived microglia

We previously reported that microglia play a central role in early sensing of HSV1 infection in the brain, and activation of host defense in mice (*12, 27*), and recently established that hiPSC-derived microglia are a powerful model system to study the antiviral immune response to herpesvirus infection (*18, 28*). The differentiation workflow from iPSCs to microglia and cortical neurons is illustrated in Figure S1A. Using bulk RNA sequencing (RNA-seq) of hiPSC-derived microglia, we found that HSV1 infection profoundly altered microglial gene expression, with a large proportion of the genes being affected (Figure S1B-C, Table S1). A broad panel of antiviral and proinflammatory genes were significantly upregulated (Fig. 1A-B). Gene ontology analysis suggests this response to impact on various processes, most notably antiviral response, leukocyte cell-cell interactions, and T cell activation (Fig. 1C). However, we also noted that a subset of the genes annotated to "response to virus" were downregulated (Fig. S1C), and this included a panel of ISGs, which were either down- or only modestly upregulated (Fig. S1D). To explore whether some of the downregulated genes were functionally related, we performed STRING analysis of the 200 most downregulated genes (Table S2). The analysis suggested four interaction nodes in this group of transcripts (Fig. 1D). One of these included several components of the TREM2 pathway, including *TREM2*, *TYROBP* (*DAP12*), *APOE*, and *SYK*. Collectively, HSV1 strongly activates antiviral transcription programs in human microglia, but also inhibits a subset of transcripts, including mRNAs encoding multiple components of the TREM2 pathway.

HSV1 infection downregulates microglial TREM2 expression in hiPSC-derived microglia

We confirmed that TREM2 expression is significantly reduced in HSV1-infected microglia (Fig. 2). The levels of cellular full-length TREM2 protein as well as both of the proteolytic cleavage TREM2 products, *i.e.*, the C-terminal fragment and secreted sTREM2, decreased substantially in cultures with HSV1-infected microglia (Fig. 2A-C). *TREM2* mRNA decreased in a virus dose-dependent and time-dependent manner (Fig. 2D-E). We observed this down-regulation with different HSV1 strains and in microglia differentiated from a separate iPSC line (Fig. S2A-C). In contrast to TREM2, and confirming the RNA sequencing data, several other central microglial genes were not affected (*MERTK*, *AXL*) or were upregulated (*TMEM119*, *P2YR12*) during HSV1 infection (Fig. S2D-E and S2F-G). To characterize the viral requirements for down-regulation of TREM2 expression, we blocked viral replication using acyclovir treatment of cells or UV treatment of the virus. Acyclovir did not alter HSV1-induced *TREM2* downregulation (Fig. 2F), whereas UV-inactivated HSV1 had lost the ability to alter *TREM2* expression levels (Fig. 2G). To test if HSV1 infection affects *TREM2* RNA stability, we used Actinomycin D to block mRNA synthesis. Indeed, *TREM2* mRNA decay occurred notably faster in the presence of HSV1 (Fig. S2H). The virion host shutoff gene (UL41) of HSV1 encodes a virion component that induces degradation of specific host mRNAs. We observed only a slight rescue of *TREM2* expression when using the ΔUL41 HSV1 mutant compared with wildtype HSV1 (Fig. S2I), suggesting that RNA degradation via this pathway is not the major mechanism exerting TREM2 downregulation. Finally, we confirmed a substantial downregulation of *TYROBP (DAP12)* mRNA and DAP12 protein (Fig. 2H-I), thus validating the RNA sequencing data showing viral targeting of several components of the TREM2 pathway.

HSV1 induces innate immune responses through the cGAS-STING pathway in human iPSC-derived microglia

As expected, HSV1 infection strongly induced *IFNB*, *IL6*, *TNFA*, and the ISG *MX1* in hiPSC-derived microglia (Fig. 2J). We have previously shown in mice that microglia sense HSV1 infection in the CNS through the cGAS-STING pathway to activate the antiviral program including type I IFNs (*9*, *12*). Here, we demonstrated that this is also the case in human microglia. Knockdown of *cGAS* substantially impaired HSV1 sensing as shown by decreased phosphorylation of STING, TBK1, and IRF3 in response to HSV1 infection (Fig. 2K and S3D). Consequently, stimulation of *IFNB*, *IL6*, *TNFA*, and *MX1* was markedly impaired (Fig. 2L). Taken together, we observed robust downregulation of TREM2 protein and mRNA in HSV1-infected human microglia and showed that the cGAS-STING pathway is essential for activating the antiviral program in human microglia.

Depletion of microglial TREM2 expression impairs the innate immune response to HSV1 infection in hiPSC-derived microglia

To determine the role of TREM2 during early HSV1 infection in hiPSC-derived microglia, we depleted *TREM2* using RNAi. The knockdown efficiency for full-length TREM2 was ~75% (Fig. 3A-C and S3A), and sTREM2 was significantly decreased as well (Fig. S3B). We did not observe a difference in cell viability in TREM2 KD cells compared with controls (Fig. 3D). To determine whether the innate immune response to HSV1 infection is affected by TREM2 knockdown (TREM2 KD), we measured mRNA levels of *IFNB*, *IL6*, *TNFA*, and *MX1* (Fig. 3E). Strikingly, we observed a significantly decreased innate immune response in TREM2-depleted microglia. Similar results were found with microglia differentiated from a separate iPSC line (Fig. S3C). Accordingly, we found impaired activation of the cGAS-STING pathway as shown by decreased phosphorylation of STING, TBK1, and IRF3 (Fig. 3F and S3D). As sTREM2 has been suggested to exert biological functions such as protection against amyloid pathology (*29*), we then tested whether replenishing sTREM2 might be able to compensate for the loss of TREM2. Treatment with sTREM2 had no effect on *IFNB* or *MX1* but induced the pro-inflammatory cytokines *IL6* and *TNFA* (Fig. S4A-C) as shown previously (*30*). Likewise, in the presence of HSV1 infection, we observed only a small increase in *TNFA* (Fig. S4D), suggesting that the decrease in sTREM2 during infection did not account for the effects observed.

Microglial protection against viral infection also involves phagocytosis of infected cells, especially neurons. To determine whether phagocytosis was impaired in TREM2-depleted microglia, we analyzed microglial phagocytosis of HSV1-infected neurons. Indeed, addition of fluorescently labeled HSV1-infected neurons to control microglia led to a prominent vesicular staining pattern (Fig. 3G, upper panel), whereas much less staining and fewer phagocytosing cells were observed in *TREM2* KD microglia (Fig. 3G, middle panel). No signal was observed in the negative control (Fig. 3G, lower panel). We further quantified the phagocytosis of HSV1-infected neurons using flow cytometry and found a significant decrease in the percentage of phagocytosed cells in TREM2 KD microglia (Fig. 3H). The phagocytosis inhibitor cytochalasin D, almost completely blocked the phagocytosis of HSV1-infected neurons, indicating that phagocytosis is necessary for entry of infected neuron debris into microglia. As expected, decreased phagocytosis of apoptotic neurons was observed in TREM2 KD microglia (Fig. 3I), whereas the phagocytosis of *E. coli* beads did not differ between control and TREM2 KD (Fig. 3J). As reported previously (*31*), this suggests a substrate-specific role of TREM2 in microglial phagocytosis and reveals that HSV1-infected neurons are phagocytosed in a TREM2-dependent manner. Together, these results show that the

antiviral response in TREM2-depleted microglia is affected in several ways, including impaired IFNB induction via the cGAS-STING pathway, and clearance of infected neurons.

TREM2 is essential for control of HSV1 infection *in vitro* and *in vivo*

HSV1 is a neurotropic virus, and in the CNS replication occurs predominantly in neurons. To investigate whether the impaired immune response in *TREM2* KD microglia affects the control of HSV1 infection *in vitro*, we co-cultured hiPSC-derived cortical neurons and microglia (Fig. S1A). As reported previously in mice (*12*), we observed that human microglia are potent producers of type I IFN (Fig. S5A). As in microglia cultures, *TREM2* mRNA as well as secreted sTREM2 protein levels were significantly decreased in HSV1-infected co-cultures (Fig. 4A and 4B). Interestingly, less viral replication and higher cell viability were observed in co-cultures compared with neurons alone (Fig. S5B and S5C). Importantly, significantly higher viral replication occurred in TREM2-depleted co-cultures, which was accompanied by decreased cell viability (Fig. 4C and 4D).

To explore whether the phenomenon observed in human microglia was also observed in mice, we infected mouse brain cells *in vitro* or live animals through the corneal route, the latter leading to infection in the brain stem. Importantly, we observed HSV1-induced *Trem2* downregulation in primary mouse microglia and in the brainstem of HSV1-infected wildtype (WT) mice (Fig. 4E and 4F). *Trem2* expression was not detected in astrocytes or neurons (Fig. 4E). *In vivo*, HSV1 infection significantly increased *Iba1* mRNA expression in the brain stem (Fig. 4I) and induced elevation in the number of cells positive for Iba-1 as well as cleaved caspase-3 (CC3), a marker of apoptosis (Fig. 4G). Furthermore, we found that HSV1 infection induced CD68 which is highly expressed by activated microglia (Fig. 4H). TREM2+ cells were abundantly present in the areas with HSV-1 infection, and some of these cells contained virus (Fig. S5D). To determine whether TREM2 is essential for control of HSV1 infection *in vivo*, we compared viral load in WT versus *Trem2*$^{-/-}$ mice. Consistent with the data from the human co-culture system, we observed significantly increased levels of infectious virus and viral mRNA in the brainstem of HSV1-infected *Trem2*$^{-/-}$ mice compared with WT (Fig. 4J and 4K). We did not detect differences in *Iba1* expression in the brain stem between genotypes, suggesting that the observed infection phenotype was unlikely to be due to a difference in microglia frequency (Fig. 4I). Collectively, these findings suggest that TREM2 depletion leads to impaired control of HSV1 infection *in vitro* and *in vivo*.

TREM2-depleted microglia respond normally to cGAMP

As we observed impaired activation of the cGAS-STING pathway by HSV1 in TREM2-depleted microglia (Fig. 3F and S3D), we wanted to test the functionality of this viral sensing pathway. To this end, we stimulated microglia with cyclic-GMP-AMP (cGAMP), which directly activates STING. Interestingly, we found no significant difference in mRNA levels of *IFNB*, *IL6*, *TNFA*, and *MX1* in cGAMP-stimulated control *versus* TREM2-depleted microglia (Fig. 5A). Accordingly, we did not observe a difference in phosphorylation of STING, TBK1, and IRF3 in cGAMP-stimulated control *versus* TREM2-depleted microglia (Fig. 5B and S6A). Also, we found no difference in *cGAS* mRNA or cGAS protein expression between control and TREM2 KD microglia (Fig. 5C-D). In addition, we observed that HSV1-induced cGAMP accumulation in microglia was not affected by knock-down of TREM2 (Fig. 5E), whereas STING phosphorylation at S366 was reduced (Fig. 3F). In uninfected cells, cGAMP was below detection limit which was

more than 15 times lower than HSV1-induced cGAMP accumulation (Fig. 5E). These results suggest that cGAS-STING signaling is not intrinsically impaired in TREM2 KD microglia, but specifically in HSV1-infected cells, and this manifests in impaired activation of the pathway between cGAMP production and STING phosphorylation.

Modulation of TREM2 activity via SYK modulates the innate immune response to HSV1 infection in microglia

The protein kinase SYK, which is an immediate downstream target of TREM2, has been shown to be crucial for STING-mediated IFN induction by HSV1 (*32*). To determine whether TREM2 might affect the antiviral immune response via SYK, we modulated TREM2 signaling and SYK activity. First, we used a TREM2-activating antibody (AF1828), which induces downstream signaling via SYK activation. As microglia express Fc receptors, IgG was used as an isotype control. As previously reported (*33*), stimulation of human microglia with the AF1828 antibody rapidly induced SYK phosphorylation in control but not in TREM2 KD cells (Fig. 6A). Using this approach, we observed that stimulation with AF1828 amplified the early immune response to HSV1 infection, as shown by significantly increased levels of *IFNB*, *IL6*, *TNFA*, and *MX1* (Fig. 6B). Likewise, TREM2 overexpression boosted the early immune response to HSV1 infection, as shown by significantly increased levels of *IFNB*, *IL6*, *TNFA*, and *MX1* (Fig. 6C-D). Next, we blocked TREM2 downstream signaling using a selective SYK inhibitor (ER27319) (Fig. 6E-F). In the presence of ER27319, SYK phosphorylation was substantially decreased upon stimulation with AF1828 (Fig. 6E). Accordingly, we found significantly decreased levels of *IFNB*, *IL6*, *TNFA*, and *MX1* upon SYK inhibition in HSV1-infected microglia (Fig. 6F), as well as impaired activation of the cGAS-STING pathway, as shown by nearly absent phosphorylation of STING, TBK1, and IRF3 (Fig. 6G). In addition, we observed that HSV1 treatment itself induced a transient SYK phosphorylation in microglia (Fig. 6H-I). Collectively, these results show that SYK activation downstream of TREM2 augments the antiviral response in microglia.

DISCUSSION

In this study we report that HSV1 actively downregulates the microglial receptor TREM2, and that this receptor plays an important role in full induction of the cGAS/STING-mediated IFN-I response to HSV1 infection. Depletion of TREM2 expression impaired the innate immune response to HSV1 infection, including type I IFN induction, and consequently promoted viral replication in human brain cell cultures and in mice. These data further support the idea of the essential role for microglia in early antiviral defense and provide mechanistic insight into the virus-cell interactions that govern the outcome of HSV1 infection in the brain.

Using bulk RNA sequencing, we found that HSV1 infection strongly induced antiviral and proinflammatory genes but also inhibited a subset of transcripts, including multiple components of the TREM2 pathway. In support of a role for TREM2 in the antiviral response, we found a dramatic decrease in the HSV1-induced activation of type I IFNs and ISGs in TREM2 KD microglia. Conversely, activation of TREM2 using an agonistic antibody or overexpression of TREM2, significantly elevated the antiviral immune response. Even though we found that HSV1 infection robustly downregulates microglial TREM2 expression, we observed substantial differences between control and TREM2 KD microglia in terms of antiviral defense mechanisms. These results indicate that TREM2 is essential for the immediate response to infection, and that the virus seeks to target this response. This is in line with previous reports suggesting that the very

early microglial immune response is crucial for control of HSV1 infection (*7-9, 12*). We did not explore other downregulated pathways, which were identified through RNA sequencing data analysis. However, it is interesting that two integrin-involving pathways were modulated by the virus, since integrins are important for the ability of microglia to migrate to sites of damage in the brain (*34*).

Herpesviruses encode a large number of genes involved in modulating cellular activities, and thus facilitate establishment and maintenance of infection. Central for these activities is the inhibition of host gene transcription during productive infection. In the human microglia, we found that HSV1 infection led to decreased stability of *TREM2* RNA. To identify the mechanism would be of clinical relevance since it may reveal potential drug targets. Using acyclovir to block viral DNA replication and post-genome replication mRNA transcription, and UV inactivation of HSV1 to block all viral genome activity, we found that downregulation of TREM2 requires active viral particles and occurs prior to viral DNA replication. Since productive HSV1 replication is rather limited in microglia, this may not be surprising. This was partially dependent on the HSV1 RNase viral host shutoff protein UL41, but the majority of the viral activity is not explained by the present data. Interestingly, in a recent phase-II pilot trial sTREM2 levels increased with valacyclovir administration in individuals with early-stage AD (*35*). In addition, TREM2 expression is also regulated by HIV, another virus with neurotropic properties (*25, 26*). This suggests that TREM2 might be targeted by various viruses and the functional consequences require further investigations.
Our data demonstrate that it is not a "dead end" for HSV1 to enter microglia, although these cells cannot be productively infected. Rather, this interaction can impair the antiviral IFN-I response, and hence promote the replication of virus that has entered more permissive cells, such as neurons.

As the primary immune cells of the brain, microglia recognize and remove injured and apoptotic cells. In our *in vitro* assay, phagocytosis of HSV1-infected neurons was found to be dependent on TREM2. Similar results have previously been reported for microglial phagocytosis of apoptotic neurons (*36-38*). HSV-infected neurons do not abundantly undergo apoptosis (*39*), and these data therefore illustrate how a range of different ligands can trigger TREM2-driven phagocytosis. In addition, the data from co-culture and *in vivo* studies identified TREM2 as an important player in the control of HSV1 infection and spread in the brain. The observed effects of TREM2 loss-of-expression are likely a combination of impaired innate immune response, decreased clearance of infected neurons and impaired recruitment of microglia to infected areas. It has been suggested that rapid recruitment of microglia is crucial to limit viral spread (*8*), and TREM2 deficiency has been demonstrated to impair chemotaxis and microglial responses to neuronal injury (*40*). Whether this also applies to HSV1-infected neurons requires further investigations.

We and others have previously shown in mice that the cGAS-STING pathway is essential for viral sensing and control of HSV1 infection in microglia (*9, 12, 41*). Here, we show that in hiPSC-derived microglia, *cGAS* depletion substantially impaired HSV1 sensing and immune activation. Strikingly, these same pathways were also impaired in TREM2 KD microglia. Using cGAMP as pathway agonist, we found that TREM2 is not intrinsically involved in STING signaling. Instead, TREM2 augments HSV1-induced cGAS-STING signaling down-stream of cGAMP production, and upstream of STING phosphorylation. Activation of SYK, which is initiated by TREM2-ligand interactions, has recently been shown to be required for STING-mediated IFN induction by HSV1

in different cell lines (*32*), and also to drive STAT1 activation in response to infection with RNA viruses (*42*). In hiPSC-derived human microglia we observed that HSV1 infection led to rapid phosphorylation of SYK, and treatment with the SYK inhibitor ER27319 diminished the antiviral IFN immune response to HSV1 infection, which we found mainly to proceed through the cGAS-STING pathway. We therefore propose that TREM2 engagement on microglia by HSV1 or HSV1-infected cells triggers SYK activation, thus amplifying signaling through the cGAS-STING pathway by augmenting STING activity dependent on its phosphorylation on S366 (Fig. 6J). Upon viral entry into microglia this response was blunted by down-regulation of *TREM2* mRNA levels, which consequently impairs the immediate antiviral host response. Recently, it has been demonstrated that hypofunctional TREM2 can be rescued by stimulating CLEC7A, a receptor that directly activates SYK, with an agonistic antibody (*43*). CLEC7A and potentially other receptors are potential therapeutic targets to boost microglial activation when TREM2 is impaired. This might be beneficial for HSV1 infection, but also other pathological brain conditions like AD.

HSV1 infection has been epidemiologically associated with development of AD, primarily in carriers of the *APOE ε4* allele (*44*). AD is the most common form of dementia and affects more than 10% of people over the age of 65 (*45*). The majority of genetic AD risk factors are implicated in microglial and innate immune cell functions (*46*), including a hypo-functional TREM2 allele which increases the AD risk several fold (*23, 24*). It is therefore tempting to speculate that the HSV1-induced downregulation of TREM2 might promote or aggravate AD-related pathologies, especially amyloid plaque accumulation. Recent data highlight a role for TREM2 in activating and directing microglial responses in disease (*47*) and controlling the ability of microglia to surround, contain, or clear Aβ (*48, 49*). Thus, microglial activation plays beneficial roles in prevention of AD, and impaired microglial activation results in a increased risk for AD. Interestingly, TREM2 has also been demonstrated to be crucial for microglia-mediated refinement of synapses in mice (*50*), thus highlighting another potential consequence of HSV1-mediated down-regulation of TREM2 expression. Given the growing interest in development of TREM2 activating antibodies as a potential therapeutic approach for AD (*51, 52*), additional insights into TREM2 function add valuable information. Immune activation to infection is essential for eventual control of virus infection in the brain. However, the brain damage that occurs during HSE is caused by both viral replication and excessive inflammatory response (*53*). Our results suggest that elevating TREM2 function might be beneficial during acute HSV1 infection in the brain, but also provide a possible mechanism for how viral reduction of TREM2 expression could affect Aβ pathology and accelerate disease processes.

The present work is mainly based on work in iPSC-derived human microglia and neurons, and in mice *in vivo*. Therefore, it does not demonstrate the relevance of the findings under natural infection in the human brain. This will require further studies, including exploration of the association of genetic variants of TREM2 with HSV1 infection in the brain. On the mechanistic level, it is a limitation of our work that the molecular mechanisms of viral destabilization of *TREM2* mRNA, and of viral activation of TREM2-SYK signaling were not fully explained. Interestingly, DNA, different lipids, and complex carbohydrates, which are present on viral particles and stressed cells, have been reported as TREM2 agonists (*19*), and further studies are needed to uncover the HSV1-microglia interactions in more detail.

Taken together, we here demonstrate that the TREM2 pathway is downregulated by HSV1 infection in microglia, and that this innate immune pathway plays a central part in the early antiviral immune response to HSV1 infection in the brain. Therefore, specific immunomodulatory strategies combined with antiviral therapy represent a promising path for better control of this devastating disease and for maintenance of brain integrity.

MATERIALS AND METHODS

Viruses and reagents

A neurovirulent clinical HSV strain was used for most *in vitro* experiments unless indicated otherwise: HSV1 2762 was isolated from the brain of a patient with fatal HSE during a clinical trial of acyclovir treatment (*54*). In addition, a KOS wildtype and a KOS mutant strain (ΔUL41) were used. For *in vivo* and primary murine cell *in vitro* experiments, the McKrae strain was used. The titers of the stocks used were determined by plaque assay on Vero cells (ATCC). AF1828 was from R&D, control IgG was from Santa Cruz (sc-2028), 2′-3′cGAMP was from InvivoGen, human recombinant sTREM2 was from Sino Biological, and Acyclovir was from Pfizer.

Generation of human hiPSC-derived microglia

Two human iPSC lines WTSIi015-A (EBiSC through Sigma-Aldrich) and ChiPSC22 (Takara Bio Europe) were used. WTSIi015-A iPS cells were used for most experiments unless indicated otherwise. IPS cells were maintained on Matrigel (Corning) in mTeSR1+ medium (Stemcell Technologies). IPSC colonies were dissociated into single cells using TrypLE Express (Thermo Fisher Scientific). Per AggreWell 800 (Stemcell Technologies) 24-well plate, $4*10^6$ iPSCs were seeded in 2 ml embryonic body medium (EBM). EBM consisted of mTeSR1+ medium supplemented with 10 µM ROCK inhibitor, 50 ng/ml BMP-4, 20 ng/ml SCF, and 50 ng/ml VEGF-121 (all from Peprotech). Cells were cultured for 4 days in Aggrewells to form embryonic bodies (EBs) with half media change (1 ml) every day. EBs were harvested using an inverted cell strainer (40 µm), and around 15 EBs were plated per 6-well in hematopoietic medium (HM). HM consisted of X-VIVO 15 medium (Lonza) supplemented with 2 mM Glutamax, 100 U/ml penicillin, 100 µg/ml streptomycin, 55 µM β-mercaptoethanol, 100 ng/ml human M-CSF (Peprotech), and 25 ng/ml human IL-3 (Peprotech). Every 7 days 2 ml media were replaced by fresh HM. After around 30 days, primitive macrophage precursors could be harvested during the media change and plated in microglia medium (MiM) at a density of 10^5 cells/cm^2. MiM consisted of Advanced DMEM F12 medium (Gibco) supplemented with 2 mM Glutamax, 100 U/ml penicillin, 100 µg/ml streptomycin, 55 µM β-mercaptoethanol, 100 ng/ml human IL-34 (Peprotech), and 10 ng/ml human GM-CSF (Peprotech). Finally, cells were differentiated in MiM for 6-9 days with full media change every other day.

Generation of human hiPSC-derived cortical neurons

One day prior to neuronal induction, WTSIi015-A iPS cells were passaged using EDTA (Thermo Fisher Scientific) and pooled 2:1. The following day, medium was switched to neural maintenance media (NMM). NMM consisted of DMEM/F12 and neurobasal media (1:1) supplemented with 1x N2 supplement, 1x B27 supplement, 50 µM 2-mercaptoethanol, 0.5x non-essential amino acids, 100 µM L-glutamine (all from Life Technologies), 2500 U/ml penicillin/streptomycin (GE Healthcare), 10 µg/ml insulin and 0.5 mM sodium pyruvate (both from Sigma-Aldrich). NMM

was further supplemented with 500 ng/ml mouse Noggin/CF chimera (R&D Systems) and 10 µM SB431542 (Stemcell Technologies). The cells were maintained in NMM for 10-12 days. The cells were then dissociated in colonies using 10 mg/ml Dispase II (Thermo Fisher Scientific) and seeded on laminin-coated plates (1-2 µg/cm^2; Sigma-Aldrich) in NMM supplemented with 20 ng/ml FGF2 (Peprotech). The cells were kept in FGF2-supplemented medium for 4 to 5 days and then further passaged with dispase two times before day 25. After 25 days, the colonies were passaged and expanded using StemPro Accutase (Thermo Fisher Scientific) until day 35. Cells can be frozen between day 25-30. On day 35, the cells were passaged a last time onto plates coated with 1-2 µg/cm2 laminin at a density of $5*10^4$ cells/cm^2 in NMM. The cells were then cultured for 2 weeks before they were used for experiments or the start of co-cultures with hiPSC-derived microglia.

Co-culture of hiPSC-derived microglia and hiPSC-derived cortical neurons

Primitive macrophage precursors, harvested during media change, were directly added to hiPSC-derived cortical neurons at a density of $2.5*10^4$ cells/cm^2. After 1 hour, media was changed to co-culture media (CoM). CoM consisted of DMEM/F12 and neurobasal media (1:1) supplemented with 1x N2 supplement, 2 mM Glutamax, 100 U/ml penicillin, 100 µg/ml streptomycin, 55 µM β-mercaptoethanol, 100 ng/ml human IL-34, and 10 ng/ml human GM-CSF. Cells were co-cultured for 2 weeks with full media change every second day.

TREM2 overexpression

The human iPSC line WTSIi015-A was used for TREM2 overexpression. Cells were grown in 6-well plates and transduced 1 ml mTESR+ with lentiviral particles (MOI 5) containing an expression plasmid for TREM2 (LPP-A3422-Lv105; GeneCopoeia). To increase transduction efficiency, 5 µg/ml polybrene was added. After 6h, an additional 1 ml of mTESR+ was added. Two days after transduction, selection was started using 0.5 µg/ml puromycin. Cells were subsequently passaged, and single cell clones were analyzed for transgene expression. A few clones were selected and used for generation of human hiPSC-derived microglia. To compensate for potential clonal effects, data from two separate clones were pooled.

siRNA-mediated knockdown

Human hiPSC-derived microglia were transfected with Lipofectamine RNAiMAX reagent (Life Technologies) according to the manufacturer´s protocol. A final siRNA concentration of 200 nM was used. Cells were used for experiments on day 4 after transfection. The following Silencer siRNAs (Ambion) were used: control (siRNA ID: 4390843), TREM2 (siRNA ID: 289814) and cGAS (siRNA ID: 129127).

Mice

C57BL/6 (WT) and *Trem2*$^{-/-}$ mice were bred at the University of Aarhus (Denmark). *Trem2*$^{-/-}$ mice were purchased from the Jackson Laboratory. Isoflurane (Abbott) or a mixture of ketamine (MSD Animal Health) and xylazine (Rompun Vet) were used to anesthetize mice. All described animal experiments have been reviewed and approved by the Danish government authorities and hence comply with Danish laws (ethics approval Nr. 2016−15−0201−01085). All efforts were made to minimize suffering and mice were monitored daily during infection. The mice were not randomized, but after HSV1 infection, information about mouse strain and treatment was blinded to the investigators. No animals were excluded from the analysis. Chow and water were provided ad libitum.

Murine ocular and HSV1 infection model

Age matched, 6 to 7-week-old male mice were anesthetized with intraperitoneal injection of a mixture of ketamine (100 mg/kg body weight) and xylazine (10 mg/kg body weight). We tested male and female mice and did not find any sex differences in any of the readouts used in the current study. Both corneas were scarified in a 10 × 10 crosshatch pattern with a 25 gauge needle and mice inoculated with HSV1 (strain McKrae, the dosage used is indicated in the figure legends) in 5 µl of infection medium (DMEM containing 200 IU ml-1 penicillin and 200 mg ml-1 streptomycin), or mock-infected with 5 µl of infection medium.

PFU assay

Vero cells (ATCC) were used for plaque assays and maintained in MEM containing 5% FBS, 1% penicillin, and 1% streptomycin. Vero cells were incubated with serial dilutions of cell supernatants. After 1 h, 0.75 % Methylcellulose (Sigma) was added, and plates were incubated at 37°C. After 3 days, the plaques were stained and counted under the microscope.

Mouse brainstems were isolated and immediately put on dry ice. Brainstems were then homogenized in DMEM and pelleted by centrifugation at 1600 ***g*** for 30 min. Supernatants were used for plaque assay as described (*12*).

sTREM2 ELISA

sTREM2 was measured using an in-house electro-chemiluminescent assay on the MESO QuickPlex SQ 120 instrument (MesoScale Discovery, USA) using a method developed by Kleinberger et al. (*55*) with modifications by Alosco *et al.* (*56*). Briefly, the capture antibody was biotinylated polyclonal goat anti-human TREM2 (0.25 µg/ml, R&D Systems), and the detector antibody was monoclonal mouse anti-human TREM2 (1 µg/ml, Santa Cruz Biotechnology). A standard curve for calculations of unknowns was constructed using recombinant human TREM2 (4000–62.5 pg/ml, Sino Biological), and samples were diluted 1:4 before being assayed

RNA isolation, RT-PCR, and qPCR

Tissues were homogenized with steel beads (Qiagen) in a Tissuelyser (II) (Qiagen) in PBS and immediately used for RNA isolation. RNA from mouse brainstem or primary cell cultures was isolated using the High Pure RNA Isolation Kit (Roche). HiPSC-derived cells were lysed in RLT Plus buffer (Qiagen) supplemented with 4 mM DTT (Sigma) and RNA was isolated using the RNeasy Mini Kit (Qiagen). cDNA was synthesized using the High-capacity cDNA Kit (Thermo Fisher Scientific).

Quantitative PCR was performed using the following TaqMan Gene Expression Assays (Applied Biosystems): *Actb* (Mm00607939_s1), *Trem2* (Mm04209424_g1), *Iba1* (Mm Mm00479862_g1), *ACTB* (Hs01060665_g1), *18S* (Hs03003631_g1), *TREM2* (Hs00219132_m1), *IFNB* (Hs01077958_s1), *IL6* (Hs00174131_m1), *TNFA* (Hs00174128_m1), *MX1* (Hs00895598_m1), and *cGAS* (Hs00403553_m1). For human *HSV1 gB* the following custom TaqMan primers and probe were used: forward primer 5′-GCAGTTTACGTACAACCACATACAGC-3′, reverse primer 5′-AGCTTGCGGGCCTCGTT-3′, and probe 56-FAM/CGGCCCAACATATCGTTGACATGGC/3BHQ_1 (IDT). For mouse *HSV1 gB* the following custom TaqMan primers and probe were used: forward primer (5′-CGCATCAAGACCACTCCTC-3′), reverse primer (5′-AGCTTGCGGGCCTCGTT-3′), and probe (5′-CGGCCCAACATATCGTTGACATGGC-3′). mRNA levels of interest were

normalized to the housekeeping gene *Actb/ACTB* or *18S* (as indicated) using the ΔΔCt method. *18S* was used as a reference gene for co-cultures, as *ACTB* expression was consistently affected by HSV1 infection.

RNA sequencing and data analysis

HiPSC-derived microglia were grown on 24-well plates at a density of $2*10^5$ cells/well and infected with HSV1 (MOI1) for 24 h. Cells were then lysed in RLT Plus buffer supplemented with 4 mM DTT. RNA was isolated using the RNeasy Micro Kit (Qiagen) including the DNA digestion step, which yielded ~1.5 µg RNA. RNA-seq including bioinformatics analysis was performed at Omiics ApS (Denmark). Samples were rRNA depleted and prepared for sequencing using SMARTer Stranded Total RNA Sample Prep Kit - HI Mammalian (Takara). Briefly, this kit first removes ribosomal RNA (rRNA) using RiboGone technology that specifically depletes nuclear rRNA sequences (5S, 5.8S, 18S, and 28S) and mitochondrial rRNA 12S. RiboGone oligos are hybridized to rRNA, which is cleaved using RNase H mediated cleavage. First strand synthesis is performed using random priming, adding an anchor for use with later PCR step. Template switching is utilized during the RT step and adds additional non-templated nucleotides to the 3' end of the newly formed cDNA. PCR is performed leveraging the non-templated nucleotides and the added anchor sequence to produce Illumina compatible libraries. Prepared libraries were quality controlled using the Bioanalyzer 2100 (Agilent) and qPCR-based concentration measurements. Libraries were equimolarly pooled and sequenced including 150 bp paired end reads on an Illumina HiSeq sequencer. Sequencing data were pre-processed by removing adapter sequence and trimming away low-quality bases with a Phred1 score below 20 using Trim Galore (v0.4.1). Quality control was performed using FastQC, Picard and MultiQC to ensure high quality data. HSV1 genome (accession code JQ673480.1) was downloaded from NCBI. The filtered RNA-seq data was mapped against the viral genome using STAR. Reads not mapping to the viral genome were extracted and mapped against the human genome (hg38 / GRCh38) using STAR and gene expression was quantified using featureCounts with gene annotations from Gencode release 38. Differential expression analysis was performed using DESeq2 package in R for human gene expression profiles.
Gene Ontology (GO) analysis was done using the clusterProfiler R package (*57*). For GO analysis all significantly differentially expressed genes (FDR < 0.05) were used except in cases were more than 3000 significant genes were found, in which case the 3000 most significant genes were used. Plotting was done in R.

STRING analysis

To identify nodes in the virus-regulated transcripts, we used the protein-protein interaction analysis tool STRING (https://string-db.org/). The proteins corresponding to the 200 most downregulated genes in the RNA-seq dataset were subjected to STRING analysis. The analysis included only physical subnetworks and a confidence of at least 0.9 was used as cut-off criteria. At least three proteins were required to qualify for a node.

Protein isolation and immunoblotting

HiPSC-derived microglia were grown on 6-well plates for protein isolation. For signaling experiments, cells were infected with HSV1 (MOI 3) for 5 hours (unless indicated otherwise). For the analysis of HSV1-regulated protein expression, cells were infected with HSV1 (MOI 1) for 24 hours. Cells were washed twice with PBS and lysed on ice for 5 min in RIPA buffer (20 mM Tris-

HCl pH 7.5, 150 mM NaCl, 1 mM EDTA, 1% Triton X-100, 0.5% sodium deoxycholate, 0.1% SDS) supplemented with protease and phosphatase inhibitor cocktails (Roche). Samples were sonicated on ice for 10 min and centrifuged at 14,000 ***g*** at 4°C for 10 min. Supernatants were collected and stored at -80°C for further use. For immunoblotting, samples were boiled at 95°C for 5 min under reducing conditions.

The following primary antibodies were used: TREM2 C-terminal (CS91068, Cell Signaling), GAPDH (CS5174), p-STING S366 (CS50907, Cell Signaling), t-STING (CS13647, Cell Signaling), p-TBK1 S172 (CS5483, Cell Signaling), t-TBK1 (CS3504, Cell Signaling), p-IRF3 S396 (CS29047, Cell Signaling), t-IRF3 (CS4302, Cell Signaling), cGAS (CS79978), beta-actin (CS3700, Cell Signaling), p-SYK Y525/526 (CS2710, Cell Signaling), t-SYK (CS13198, Cell Signaling). The following secondary antibodies were used: IRDye® 800CW donkey anti-rabbit IgG and IRDye® 680RD donkey anti-mouse IgG (both from LI-COR Biotechnology).

Immunocytochemistry

Cells grown on Ibidi µ-slides (Ibidi) were washed twice in PBS and fixed in 4% paraformaldehyde for 20 min at RT, covered with PBS and stored at 4°C until analysis. The cells were permeabilized with 0.3% Triton-X100 in TBS for 15 min at RT and incubated with blocking buffer (0.3% Triton-X100 and 5% donkey serum in TBS) for 1 h at RT. Primary antibodies were diluted in blocking buffer. The following primary antibodies were used for staining: IBA1 (ab5076, Abcam), TUJ1 (ab14545, Abcam), and TREM2 (AF1828, R&D Systems). Samples were incubated with primary antibodies overnight at 4°C. Cells were washed 3x in TBS and incubated for 1 h with secondary antibodies diluted 1:500 in blocking buffer. Cells were washed 3x in TBS, counterstained using DAPI, and mounted using Ibidi mounting media (Ibidi). Samples were imaged using a Nikon A1 inverted confocal microscope.

Immunohistochemistry

Immunohistochemistry was done as previously described (*39*). Briefly, mice were perfused and dissected brains were fixed in 4% formaldehyde, embedded in paraffin, and sections (7 µm) were cut. Sections were deparaffinized, rehydrolyzed, and antigens were retrieved for 30 min at 80°C using the Target Retrieval Solution (Darko). Sections were blocked with blocking buffer (1% BSA and 0.3% Triton X-100 in TBS) for 1 h at RT. Samples were incubated for 48 h at 4°C with the following primary antibodies: HSV-1 (1:500; B0116, Dako, Cytomation), cleaved caspase-3 (1:300; CS9661, Cell Signaling), Iba-1 (1:400; ab5076, Abcam), Trem2 (1:50; AF1729, R&D Systems). As a negative control, we used secondary antibodies alone or an isotype control if the primary antibody was monoclonal. After several washes in TBS-TX (0.3% Triton X-100 in TBS), the sections were incubated with appropriate secondary antibodies coupled to Alexa Fluor 647, 568, or 488 (1:500; Invitrogen) for 1 h at RT. Nuclei were stained with DAPI for 6 min. Finally, the sections were washed 5 times with TBS-TX and mounted with ProLong Gold. Sections were imaged on a Zeiss LSM 710, LSM 800 laser scanning microscope, and Leica Leitz DMRB fluorescence microscope. Zen 2012 acquisition software and ImageJ (NIH) were used for imaging and analysis.

cGAMP quantification

HiPSC-derived microglia were grown on 6-well plates and infected with HSV1 (MOI 1) for 24 h. Cells were washed 2x with PBS, cells were carefully scraped, cells were collected in 500 µl PBS/well and 2 wells were merged. Cells were counted and then centrifuged at 200 ***g*** for 5 min.

The supernatant was discarded and 250 µl internal standard solution (10 nM cGMP in acetonitrile:methanol [1:1]) was added to the cell pellet. Samples were vortexed and stored at -80°C until further analysis. Samples were extracted by sonication for 10 min followed by vortexing (1400 rpm) for an additional 10 min. Samples were centrifuged at 16,000 ***g*** for 10 min and supernatants were evaporated under a stream of nitrogen before reconstitution in 100 µl acetonitrile:methanol [3:1]. Quantification was performed using ultra-performance liquid chromatography coupled to tandem mass spectrometry (UPLC-MS/MS). Five µl were injected onto a Waters zHILIC column (2.1 x 100; 1.7 µM particles) and separated using a gradient of acetonitrile with 0.1% formic acid as B-phase and water with 20 mM ammonium formate as A-phase. Detection was performed on a Sciex 7500 triple quadrupole mass spectrometer (Sciex). Quantification was made against an external calibration curve with a limit of detection of 0.1 nM.

Cell viability assay

The CyQUANT XTT assay (Invitrogen) was used to measure cell viability. HiPSC-derived co-cultures were infected with HSV1 as indicated. After 24 h, 150 µl media were removed and stored at -80°C for further analyses. Sixty-five µl CyQUANT Mix were added to the remaining 100 µl and cells were incubated for 3 h. Cell supernatants were transferred to a 96-well plate and absorbance (A) was measured at 450 and 660 nm. Specific absorbance was calculated by using the formula: $A_{(450\ nm)}$-$A_{(660\ nm)}$.

Annexin V staining and FACS analysis

Annexin V-Alexa 488 conjugates (Thermo Fisher Scientific) were used for apoptosis detection according to the manufacturer's instructions. Briefly, hiPSC-derived microglia were trypsinized, washed 1x with PBS at 400 g for 5 min, and resuspended in annexin-binding buffer at $1*10^6$ cells/ml. Five µl annexin V conjugate were added per 100 µl cell solution, incubated for 15 min at RT, and 400 µl of annexin-binding buffer were added. Cells were analyzed using a FACSAria Fusion, the Annexin V conjugate signal was detected in the FITC channel, and positive cells were quantified using the BD FACSDiva software.

Phagocytosis assays

For analysis of phagocytosis of HSV1-infected neurons, hiPSC-derived neurons were infected with HSV1 (10 MOI). After 24 h, cells were washed 1x with PBS and fresh NMM was added. Cells were subjected to UV irradiation for 10 min to inactivate HSV1. Cells were then trypsinized, centrifuged at 400 g for 5 min, resuspended in PBS containing 2 µg/ml fluorescent cell tracker (CellTracker™ CM-DiI Dye, Thermo Fisher Scientific), and incubated for 5 min at 37°C. Cells were washed 2x with PBS at 400 ***g*** for 5 min. The UV inactivation of the virus was confirmed by plaque assay. Cells were resuspended in MiM and added to the cultured hiPSC-derived microglia, at a 1:1 cell ratio, for 15 h. For ICC, microglia were washed 2x with PBS and fixed in 4% paraformaldehyde for 20 min at RT followed by DAPI counterstaining and mounting. Samples were imaged using a Nikon A1 inverted confocal microscope. For FACS analysis, microglia were trypsinized, washed 2x with PBS at 400 ***g*** for 5 min, and resuspended in 200 µl PBS for FACS analysis using a FACSAria Fusion. The cell tracker signal was detected in the PE channel and positive cells were quantified using the BD FACSDiva software.

For analysis of phagocytosis of apoptotic neurons, apoptosis was induced in hiPSC-derived neurons by adding 30 nM okadaic acid to the cell media for 3 h. Neurons were trypsinized, washed 1x in PBS, resuspended in PBS containing 2 µg/ml fluorescent cell tracker, and incubated for 5

min at 37°C. Cells were washed 2x with PBS at 400 g for 5 min, resuspended in MiM, and added to the cultured hiPSC-derived microglia at a 1:10 cell ratio for 3 h. Microglia were prepared for FACS analysis as above.

For analysis of phagocytosis of pHrodo-*E. coli* beads (Thermo Fisher Scientific), beads were resuspended in live cell imaging solution (2 ml/vial of beads, Thermo Fisher Scientific) and briefly sonicated. hiPSC-derived microglia were grown in black clear bottom 96-well plates and incubated with 100 µl beads solution for 3 h. Phagocytosis of pHrodo-*E. coli* beads was quantified using a microplate reader and excitation/emission wavelengths of 560/585 nm.

To inhibit phagocytosis, cells were incubated with 5 µM Cytochalasin D (Thermo Fisher Scientific) 1 hour prior to experiments and during experiments.

mRNA stability assay

Actinomycin D, which inhibits the synthesis of new mRNA, was used for the assessment of mRNA decay. hiPSC-derived microglia were incubated with 5 µg/ml Actinomycin D for the indicated time points in presence and absence of HSV1 (MOI 3). RNA was isolated, followed by cDNA synthesis and qPCR. *TREM2* mRNA expression was quantified relative to time point 0.

Statistical analyses

For statistical analysis of data, we used two-tailed Student's *t*-test when the data exhibited normal distribution, and Mann-Whitney *U* test when the data set did not pass the normal distribution test or normal distribution could not be tested. When comparing more than two groups, multiple-comparison one-way ANOVA was used with Tukey's multiple-comparison test. All experimental data were reliably reproduced in two or more independent experiments. Individual data points represent biological replicates. GraphPad Prism 8 software and R were used for statistical analyses. No measurement was excluded for statistical analysis.

List of Supplementary Materials

Fig. S1 to S6

Table S1 to S2

References

1. K. L. Tyler, Acute Viral Encephalitis. *N Engl J Med* **379**, 557-566 (2018).
2. J. P. Stahl, A. Mailles, Herpes simplex virus encephalitis update. *Curr Opin Infect Dis* **32**, 239-243 (2019).
3. K. L. Roos, Encephalitis. *Handb Clin Neurol* **121**, 1377-1381 (2014).
4. R. G. Pebody, N. Andrews, D. Brown, R. Gopal, H. De Melker, G. Francois, N. Gatcheva, W. Hellenbrand, S. Jokinen, I. Klavs, M. Kojouharova, T. Kortbeek, B. Kriz, K. Prosenc, K. Roubalova, P. Teocharov, W. Thierfelder, M. Valle, P. Van Damme, R. Vranckx, The seroepidemiology of herpes simplex virus type 1 and 2 in Europe. *Sex Transm Infect* **80**, 185-191 (2004).
5. A. J. Steel, G. D. Eslick, Herpes Viruses Increase the Risk of Alzheimer's Disease: A Meta-Analysis. *Journal of Alzheimer's disease : JAD* **47**, 351-364 (2015).
6. R. F. Itzhaki, W. R. Lin, D. Shang, G. K. Wilcock, B. Faragher, G. A. Jamieson, Herpes simplex virus type 1 in brain and risk of Alzheimer's disease. *Lancet* **349**, 241-244 (1997).
7. O. Uyar, N. Laflamme, J. Piret, M.-C. Venable, J. Carbonneau, K. Zarrouk, S. Rivest, G. Boivin, An Early Microglial Response Is Needed To Efficiently Control Herpes Simplex Virus Encephalitis. *Journal of Virology* **94**, (2020).

8. R. Fekete, C. Cserep, N. Lenart, K. Toth, B. Orsolits, B. Martinecz, E. Mehes, B. Szabo, V. Nemeth, B. Gonci, B. Sperlagh, Z. Boldogkoi, A. Kittel, M. Baranyi, S. Ferenczi, K. Kovacs, G. Szalay, B. Rozsa, C. Webb, G. G. Kovacs, T. Hortobagyi, B. L. West, Z. Kornyei, A. Denes, Microglia control the spread of neurotropic virus infection via P2Y12 signalling and recruit monocytes through P2Y12-independent mechanisms. *Acta Neuropathol* **136**, 461-482 (2018).

9. G. Katzilieris-Petras, X. Lai, A. S. Rashidi, G. Verjans, L. S. Reinert, S. R. Paludan, Microglia activate early anti-viral responses upon HSV-1 entry into the brain to counteract development of encephalitis-like disease in mice. *J Virol*, JVI0131121 (2022).

10. L. Sun, J. Wu, F. Du, X. Chen, Z. J. Chen, Cyclic GMP-AMP synthase is a cytosolic DNA sensor that activates the type I interferon pathway. *Science* **339**, 786-791 (2013).

11. H. Ishikawa, G. N. Barber, STING is an endoplasmic reticulum adaptor that facilitates innate immune signalling. *Nature* **455**, 674-678 (2008).

12. L. S. Reinert, K. Lopusna, H. Winther, C. Sun, M. K. Thomsen, R. Nandakumar, T. H. Mogensen, M. Meyer, C. Vaegter, J. R. Nyengaard, K. A. Fitzgerald, S. R. Paludan, Sensing of HSV-1 by the cGAS-STING pathway in microglia orchestrates antiviral defence in the CNS. *Nat Commun* **7**, 13348 (2016).

13. M. Herman, M. Ciancanelli, Y. H. Ou, L. Lorenzo, M. Klaudel-Dreszler, E. Pauwels, V. Sancho-Shimizu, R. Perez de Diego, A. Abhyankar, E. Israelsson, Y. Guo, A. Cardon, F. Rozenberg, P. Lebon, M. Tardieu, E. Heropolitanska-Pliszka, D. Chaussabel, M. A. White, L. Abel, S. Y. Zhang, J. L. Casanova, Heterozygous TBK1 mutations impair TLR3 immunity and underlie herpes simplex encephalitis of childhood. *J Exp Med* **209**, 1567-1582 (2012).

14. L. L. Andersen, N. Mork, L. S. Reinert, E. Kofod-Olsen, R. Narita, S. E. Jorgensen, K. A. Skipper, K. Honing, H. H. Gad, L. Ostergaard, T. F. Orntoft, V. Hornung, S. R. Paludan, J. G. Mikkelsen, T. Fujita, M. Christiansen, R. Hartmann, T. H. Mogensen, Functional IRF3 deficiency in a patient with herpes simplex encephalitis. *J Exp Med* **212**, 1371-1379 (2015).

15. S. Pan, X. Liu, Y. Ma, Y. Cao, B. He, Herpes Simplex Virus 1 gamma134.5 Protein Inhibits STING Activation That Restricts Viral Replication. *J Virol* **92**, (2018).

16. J. Huang, H. You, C. Su, Y. Li, S. Chen, C. Zheng, Herpes Simplex Virus 1 Tegument Protein VP22 Abrogates cGAS/STING-Mediated Antiviral Innate Immunity. *J Virol* **92**, (2018).

17. M. H. Christensen, S. B. Jensen, J. J. Miettinen, S. Luecke, T. Prabakaran, L. S. Reinert, T. Mettenleiter, Z. J. Chen, D. M. Knipe, R. M. Sandri-Goldin, L. W. Enquist, R. Hartmann, T. H. Mogensen, S. A. Rice, T. A. Nyman, S. Matikainen, S. R. Paludan, HSV-1 ICP27 targets the TBK1-activated STING signalsome to inhibit virus-induced type I IFN expression. *EMBO J* **35**, 1385-1399 (2016).

18. C. Bodda, L. S. Reinert, S. Fruhwürth, T. Richardo, C. Sun, B. C. Zhang, M. Kalamvoki, A. Pohlmann, T. H. Mogensen, P. Bergström, L. Agholme, P. O'Hare, B. Sodeik, M. Gyrd-Hansen, H. Zetterberg, S. R. Paludan, HSV1 VP1-2 deubiquitinates STING to block type I interferon expression and promote brain infection. *J Exp Med* **217**, (2020).

19. D. L. Kober, T. J. Brett, TREM2-Ligand Interactions in Health and Disease. *J Mol Biol* **429**, 1607-1629 (2017).

20. F. Filipello, C. Goldsbury, S. F. You, A. Locca, C. M. Karch, L. Piccio, Soluble TREM2: Innocent bystander or active player in neurological diseases? *Neurobiology of disease* **165**, 105630 (2022).

21. J. Paloneva, M. Kestila, J. Wu, A. Salminen, T. Bohling, V. Ruotsalainen, P. Hakola, A. B. Bakker, J. H. Phillips, P. Pekkarinen, L. L. Lanier, T. Timonen, L. Peltonen, Loss-of-function mutations in TYROBP (DAP12) result in a presenile dementia with bone cysts. *Nat Genet* **25**, 357-361 (2000).

22. J. Paloneva, T. Manninen, G. Christman, K. Hovanes, J. Mandelin, R. Adolfsson, M. Bianchin, T. Bird, R. Miranda, A. Salmaggi, L. Tranebjaerg, Y. Konttinen, L. Peltonen, Mutations in two genes encoding different subunits of a receptor signaling complex result in an identical disease phenotype. *Am J Hum Genet* **71**, 656-662 (2002).

23. R. Guerreiro, A. Wojtas, J. Bras, M. Carrasquillo, E. Rogaeva, E. Majounie, C. Cruchaga, C. Sassi, J. S. Kauwe, S. Younkin, L. Hazrati, J. Collinge, J. Pocock, T. Lashley, J. Williams, J. C. Lambert, P. Amouyel, A. Goate, R. Rademakers, K. Morgan, J. Powell, P. St George-Hyslop, A. Singleton, J. Hardy, G. Alzheimer Genetic Analysis, TREM2 variants in Alzheimer's disease. *N Engl J Med* **368**, 117-127 (2013).

24. T. Jonsson, H. Stefansson, S. Steinberg, I. Jonsdottir, P. V. Jonsson, J. Snaedal, S. Bjornsson, J. Huttenlocher, A. I. Levey, J. J. Lah, D. Rujescu, H. Hampel, I. Giegling, O. A. Andreassen, K. Engedal, I. Ulstein, S. Djurovic, C. Ibrahim-Verbaas, A. Hofman, M. A. Ikram, C. M. van Duijn, U. Thorsteinsdottir, A. Kong, K. Stefansson, Variant of TREM2 associated with the risk of Alzheimer's disease. *N Engl J Med* **368**, 107-116 (2013).

25. D. Bortolotti, V. Gentili, A. Rotola, E. Caselli, R. Rizzo, HHV-6A infection induces amyloid-beta expression and activation of microglial cells. *Alzheimer's research & therapy* **11**, 104 (2019).
26. J. A. Fields, B. Spencer, M. Swinton, E. M. Qvale, M. J. Marquine, A. Alexeeva, S. Gough, B. Soontornniyomkij, E. Valera, E. Masliah, C. L. Achim, P. Desplats, Alterations in brain TREM2 and Amyloid-beta levels are associated with neurocognitive impairment in HIV-infected persons on antiretroviral therapy. *J Neurochem* **147**, 784-802 (2018).
27. G. Katzilieris-Petras, X. Lai, A. S. Rashidi, G. Verjans, L. S. Reinert, S. R. Paludan, Microglia Activate Early Antiviral Responses upon Herpes Simplex Virus 1 Entry into the Brain to Counteract Development of Encephalitis-Like Disease in Mice. *J Virol* **96**, e0131121 (2022).
28. L. S. Reinert, A. S. Rashidi, D. N. Tran, G. Katzilieris-Petras, A. K. Hvidt, M. Gohr, S. Fruhwurth, C. Bodda, M. K. Thomsen, M. H. Vendelbo, A. R. Khan, B. Hansen, P. Bergstrom, L. Agholme, T. H. Mogensen, M. H. Christensen, J. R. Nyengaard, G. C. Sen, H. Zetterberg, G. M. Verjans, S. R. Paludan, Brain immune cells undergo cGAS/STING-dependent apoptosis during herpes simplex virus type 1 infection to limit type I IFN production. *The Journal of clinical investigation* **131**, (2021).
29. G. C. Brown, P. St George-Hyslop, Does Soluble TREM2 Protect Against Alzheimer's Disease? *Front Aging Neurosci* **13**, 834697 (2021).
30. L. Zhong, Y. Xu, R. Zhuo, T. Wang, K. Wang, R. Huang, D. Wang, Y. Gao, Y. Zhu, X. Sheng, K. Chen, N. Wang, L. Zhu, D. Can, Y. Marten, M. Shinohara, C. C. Liu, D. Du, H. Sun, L. Wen, H. Xu, G. Bu, X. F. Chen, Soluble TREM2 ameliorates pathological phenotypes by modulating microglial functions in an Alzheimer's disease model. *Nat Commun* **10**, 1365 (2019).
31. P. Garcia-Reitboeck, A. Phillips, T. M. Piers, C. Villegas-Llerena, M. Butler, A. Mallach, C. Rodrigues, C. E. Arber, A. Heslegrave, H. Zetterberg, H. Neumann, S. Neame, H. Houlden, J. Hardy, J. M. Pocock, Human Induced Pluripotent Stem Cell-Derived Microglia-Like Cells Harboring TREM2 Missense Mutations Show Specific Deficits in Phagocytosis. *Cell Rep* **24**, 2300-2311 (2018).
32. C. Wang, N. Sharma, M. Veleeparambil, P. M. Kessler, B. Willard, G. C. Sen, STING-Mediated Interferon Induction by Herpes Simplex Virus 1 Requires the Protein Tyrosine Kinase Syk. *mBio* **12**, e0322821 (2021).
33. A. McQuade, Y. J. Kang, J. Hasselmann, A. Jairaman, A. Sotelo, M. Coburn, S. K. Shabestari, J. P. Chadarevian, G. Fote, C. H. Tu, E. Danhash, J. Silva, E. Martinez, C. Cotman, G. A. Prieto, L. M. Thompson, J. S. Steffan, I. Smith, H. Davtyan, M. Cahalan, H. Cho, M. Blurton-Jones, Gene expression and functional deficits underlie TREM2-knockout microglia responses in human models of Alzheimer's disease. *Nat Commun* **11**, 5370 (2020).
34. C. Kim, E. D. Cho, H. K. Kim, S. You, H. J. Lee, D. Hwang, S. J. Lee, beta1-integrin-dependent migration of microglia in response to neuron-released alpha-synuclein. *Exp Mol Med* **46**, e91 (2014).
35. B. Weidung, E. S. Hemmingsson, J. Olsson, T. Sundstrom, K. Blennow, H. Zetterberg, M. Ingelsson, F. Elgh, H. Lovheim, VALZ-Pilot: High-dose valacyclovir treatment in patients with early-stage Alzheimer's disease. *Alzheimer's & dementia (New York, N. Y.)* **8**, e12264 (2022).
36. K. Takahashi, C. D. Rochford, H. Neumann, Clearance of apoptotic neurons without inflammation by microglial triggering receptor expressed on myeloid cells-2. *J Exp Med* **201**, 647-657 (2005).
37. P. Garcia-Reitboeck, A. Phillips, T. M. Piers, C. Villegas-Llerena, M. Butler, A. Mallach, C. Rodrigues, C. E. Arber, A. Heslegrave, H. Zetterberg, H. Neumann, S. Neame, H. Houlden, J. Hardy, J. M. Pocock, Human Induced Pluripotent Stem Cell-Derived Microglia-Like Cells Harboring TREM2 Missense Mutations Show Specific Deficits in Phagocytosis. *Cell Reports* **24**, 2300-2311 (2018).
38. C. L. Hsieh, M. Koike, S. C. Spusta, E. C. Niemi, M. Yenari, M. C. Nakamura, W. E. Seaman, A role for TREM2 ligands in the phagocytosis of apoptotic neuronal cells by microglia. *J Neurochem* **109**, 1144-1156 (2009).
39. L. S. Reinert, A. S. Rashidi, D. N. Tran, G. Katzilieris-Petras, A. K. Hvidt, M. Gohr, S. Fruhwürth, C. Bodda, M. K. Thomsen, M. H. Vendelbo, A. R. Khan, B. Hansen, P. Bergström, L. Agholme, T. H. Mogensen, M. H. Christensen, J. R. Nyengaard, G. C. Sen, H. Zetterberg, G. M. Verjans, S. R. Paludan, Brain immune cells undergo cGAS/STING-dependent apoptosis during herpes simplex virus type 1 infection to limit type I IFN production. *Journal of Clinical Investigation* **131**, (2021).
40. F. Mazaheri, N. Snaidero, G. Kleinberger, C. Madore, A. Daria, G. Werner, S. Krasemann, A. Capell, D. Trumbach, W. Wurst, B. Brunner, S. Bultmann, S. Tahirovic, M. Kerschensteiner, T. Misgeld, O. Butovsky, C. Haass, TREM2 deficiency impairs chemotaxis and microglial responses to neuronal injury. *EMBO Rep* **18**, 1186-1198 (2017).

41. Z. M. Parker, A. A. Murphy, D. A. Leib, Role of the DNA Sensor STING in Protection from Lethal Infection following Corneal and Intracerebral Challenge with Herpes Simplex Virus 1. *J Virol* **89**, 11080-11091 (2015).
42. S. Liu, Y. Liao, B. Chen, Y. Chen, Z. Yu, H. Wei, L. Zhang, S. Huang, P. B. Rothman, G. F. Gao, J. L. Chen, Critical role of Syk-dependent STAT1 activation in innate antiviral immunity. *Cell Rep* **34**, 108627 (2021).
43. S. Wang, R. Sudan, V. Peng, Y. Zhou, S. Du, C. M. Yuede, T. Lei, J. Hou, Z. Cai, M. Cella, K. Nguyen, P. L. Poliani, W. L. Beatty, Y. Chen, S. Cao, K. Lin, C. Rodrigues, A. H. Ellebedy, S. Gilfillan, G. D. Brown, D. M. Holtzman, S. Brioschi, M. Colonna, TREM2 drives microglia response to amyloid-beta via SYK-dependent and -independent pathways. *Cell* **185**, 4153-4169 e4119 (2022).
44. L. N. Zhang, M. J. Li, Y. H. Shang, F. F. Zhao, H. C. Huang, F. X. Lao, Independent and Correlated Role of Apolipoprotein E varepsilon4 Genotype and Herpes Simplex Virus Type 1 in Alzheimer's Disease. *Journal of Alzheimer's disease : JAD* **77**, 15-31 (2020).
45. 2021 Alzheimer's disease facts and figures. *Alzheimer's & dementia : the journal of the Alzheimer's Association* **17**, 327-406 (2021).
46. Y. Shi, D. M. Holtzman, Interplay between innate immunity and Alzheimer disease: APOE and TREM2 in the spotlight. *Nat Rev Immunol* **18**, 759-772 (2018).
47. H. Keren-Shaul, A. Spinrad, A. Weiner, O. Matcovitch-Natan, R. Dvir-Szternfeld, T. K. Ulland, E. David, K. Baruch, D. Lara-Astaiso, B. Toth, S. Itzkovitz, M. Colonna, M. Schwartz, I. Amit, A Unique Microglia Type Associated with Restricting Development of Alzheimer's Disease. *Cell* **169**, 1276-1290 e1217 (2017).
48. Y. Wang, T. K. Ulland, J. D. Ulrich, W. Song, J. A. Tzaferis, J. T. Hole, P. Yuan, T. E. Mahan, Y. Shi, S. Gilfillan, M. Cella, J. Grutzendler, R. B. DeMattos, J. R. Cirrito, D. M. Holtzman, M. Colonna, TREM2-mediated early microglial response limits diffusion and toxicity of amyloid plaques. *J Exp Med* **213**, 667-675 (2016).
49. S. Parhizkar, T. Arzberger, M. Brendel, G. Kleinberger, M. Deussing, C. Focke, B. Nuscher, M. Xiong, A. Ghasemigharagoz, N. Katzmarski, S. Krasemann, S. F. Lichtenthaler, S. A. Muller, A. Colombo, L. S. Monasor, S. Tahirovic, J. Herms, M. Willem, N. Pettkus, O. Butovsky, P. Bartenstein, D. Edbauer, A. Rominger, A. Erturk, S. A. Grathwohl, J. J. Neher, D. M. Holtzman, M. Meyer-Luehmann, C. Haass, Loss of TREM2 function increases amyloid seeding but reduces plaque-associated ApoE. *Nat Neurosci* **22**, 191-204 (2019).
50. F. Filipello, R. Morini, I. Corradini, V. Zerbi, A. Canzi, B. Michalski, M. Erreni, M. Markicevic, C. Starvaggi-Cucuzza, K. Otero, L. Piccio, F. Cignarella, F. Perrucci, M. Tamborini, M. Genua, L. Rajendran, E. Menna, S. Vetrano, M. Fahnestock, R. C. Paolicelli, M. Matteoli, The Microglial Innate Immune Receptor TREM2 Is Required for Synapse Elimination and Normal Brain Connectivity. *Immunity* **48**, 979-991 e978 (2018).
51. S. Wang, M. Mustafa, C. M. Yuede, S. V. Salazar, P. Kong, H. Long, M. Ward, O. Siddiqui, R. Paul, S. Gilfillan, A. Ibrahim, H. Rhinn, I. Tassi, A. Rosenthal, T. Schwabe, M. Colonna, Anti-human TREM2 induces microglia proliferation and reduces pathology in an Alzheimer's disease model. *J Exp Med* **217**, (2020).
52. K. Schlepckow, K. M. Monroe, G. Kleinberger, L. Cantuti-Castelvetri, S. Parhizkar, D. Xia, M. Willem, G. Werner, N. Pettkus, B. Brunner, A. Sulzen, B. Nuscher, H. Hampel, X. Xiang, R. Feederle, S. Tahirovic, J. I. Park, R. Prorok, C. Mahon, C. C. Liang, J. Shi, D. J. Kim, H. Sabelstrom, F. Huang, G. Di Paolo, M. Simons, J. W. Lewcock, C. Haass, Enhancing protective microglial activities with a dual function TREM2 antibody to the stalk region. *EMBO Mol Med* **12**, e11227 (2020).
53. J. Piret, G. Boivin, Immunomodulatory Strategies in Herpes Simplex Virus Encephalitis. *Clinical Microbiology Reviews* **33**, (2020).
54. B. Skoldenberg, M. Forsgren, K. Alestig, T. Bergstrom, L. Burman, E. Dahlqvist, A. Forkman, A. Fryden, K. Lovgren, K. Norlin, et al., Acyclovir versus vidarabine in herpes simplex encephalitis. Randomised multicentre study in consecutive Swedish patients. *Lancet* **2**, 707-711 (1984).
55. G. Kleinberger, Y. Yamanishi, M. Suarez-Calvet, E. Czirr, E. Lohmann, E. Cuyvers, H. Struyfs, N. Pettkus, A. Wenninger-Weinzierl, F. Mazaheri, S. Tahirovic, A. Lleo, D. Alcolea, J. Fortea, M. Willem, S. Lammich, J. L. Molinuevo, R. Sanchez-Valle, A. Antonell, A. Ramirez, M. T. Heneka, K. Sleegers, J. van der Zee, J. J. Martin, S. Engelborghs, A. Demirtas-Tatlidede, H. Zetterberg, C. Van Broeckhoven, H. Gurvit, T. Wyss-Coray, J. Hardy, M. Colonna, C. Haass, TREM2 mutations implicated in neurodegeneration impair cell surface transport and phagocytosis. *Sci Transl Med* **6**, 243ra286 (2014).

56. M. L. Alosco, Y. Tripodis, N. G. Fritts, A. Heslegrave, C. M. Baugh, S. Conneely, M. Mariani, B. M. Martin, S. Frank, J. Mez, T. D. Stein, R. C. Cantu, A. C. McKee, L. M. Shaw, J. Q. Trojanowski, K. Blennow, H. Zetterberg, R. A. Stern, Cerebrospinal fluid tau, Abeta, and sTREM2 in Former National Football League Players: Modeling the relationship between repetitive head impacts, microglial activation, and neurodegeneration. *Alzheimer's & dementia : the journal of the Alzheimer's Association* **14**, 1159-1170 (2018).
57. T. Wu, E. Hu, S. Xu, M. Chen, P. Guo, Z. Dai, T. Feng, L. Zhou, W. Tang, L. Zhan, X. Fu, S. Liu, X. Bo, G. Yu, clusterProfiler 4.0: A universal enrichment tool for interpreting omics data. *Innovation (Camb)* **2**, 100141 (2021).

Acknowledgments: We would like to thank Monica Malmberg for her help with sTREM2 immunoassays, Susann Li for her help with FACS, and Frederik Seelig for proof-reading the manuscript. We would like to acknowledge that Fig. 6J was created with BioRender.com.

Funding:
Petrus och Augusta Hedlunds Stiftelse M-2022-1825 (SF)
The European Research Council 786602 (SRP)
The Lundbeck Foundation R359-2020-2287 (SRP)
The Swedish Research Council 2018-02463 and 2021-00942 (SRP)
The Novo Nordisk Foundation NNF20OC0063436 (SRP)
Swedish Research Council 2018-02532 (HZ)
European Research Council 681712 (HZ)
European Research Council 101053962 (HZ)
Swedish State Support for Clinical Research ALFGBG-71320 (HZ)
Alzheimer Drug Discovery Foundation 201809-2016862 (HZ)
Alzheimer's Association ADSF-21-831376-C (HZ)
Alzheimer's Association ADSF-21-831381-C (HZ)
Alzheimer's Association ADSF-21-831377-C (HZ)
Hjärnfonden FO2019-0228 (HZ)
European Union’s Horizon 2020 research and innovation programme under the Marie Skłodowska-Curie grant agreement 860197 (HZ)
European Union Joint Programme-Neurodegenerative Disease Research JPND2021-00694 (HZ)
UK Dementia Research Institute at UCL UKDRI-1003 (HZ)

Author contributions:
Conceptualization: SF, SRP, LSR, HZ
Methodology: SF, LSR, MH
Investigation: SF, LSR, CÖ, MS, MH
Visualization: SF
Funding acquisition: SRP, HZ, SF
Supervision: SF, SRP, HZ
Writing – original draft: SF, SRP
Writing – review & editing: SF, SRP, HZ, LSR, CÖ, MS, MH

Competing interests: HZ has served at scientific advisory boards and/or as a consultant for Abbvie, Alector, ALZPath, Annexon, Apellis, Artery Therapeutics, AZTherapies, CogRx, Denali, Eisai, Nervgen, Novo Nordisk, Pinteon Therapeutics, Red Abbey Labs, reMYND, Passage Bio, Roche, Samumed, Siemens Healthineers, Triplet Therapeutics, and Wave, has given lectures in symposia sponsored by Cellectricon, Fujirebio, Alzecure, Biogen, and Roche, and is a co-founder of Brain Biomarker Solutions in Gothenburg AB (BBS), which is a part of the GU Ventures Incubator Program (outside submitted work). The authors declare no other competing interests.

Data and materials availability: All data are available in the main text or the supplementary materials.

Figures

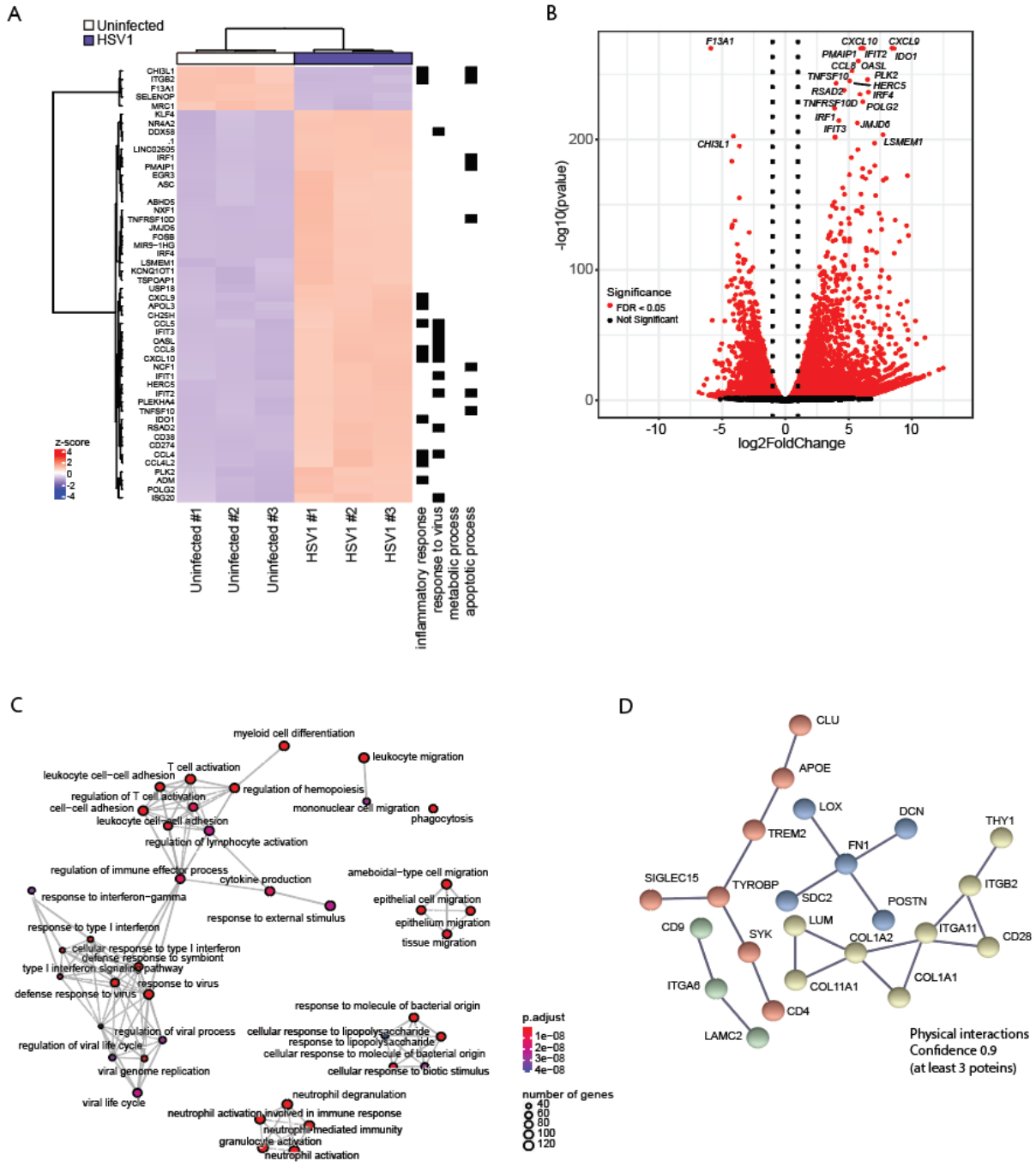

Fig. 1. **RNA-seq of HSV1-infected microglia.** (**A-D**) hiPSC-derived microglia were infected with HSV1 (MOI 1) for 24 h. (**A**) Hierarchical clustering of genes differentially expressed in HSV1- versus uninfected microglia. Top 50 genes are shown. Biological function annotated with the regulated genes shown to the right. (**B**) Volcano plot of differentially expressed genes in uninfected versus HSV1-infected microglia (red, false-discovery rate [FDR] < 0.05). The top 20 differentially regulated genes are indicated. (**C**) Gene ontology enrichment plot in the category biological processes of the top 50 differentially expressed genes. (**D**) Network representation of the protein-

protein interactions of the 200 most downregulated genes using STRING analysis. Nodes are represented with different colors for each node.

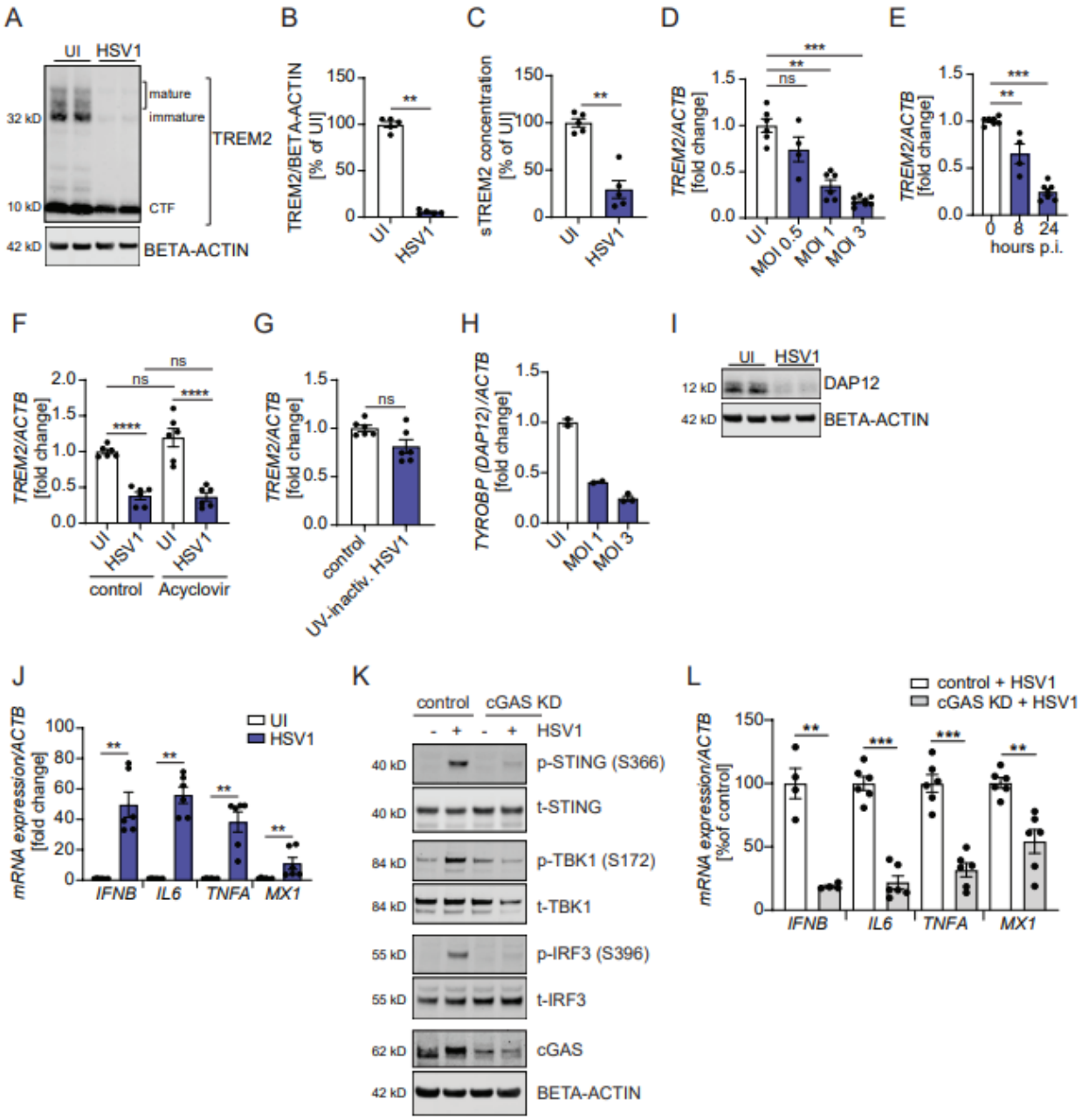

Fig. 2. HSV1 downregulates microglial TREM2 expression. (**A**-**C**) hiPSC-derived microglia were infected with HSV1 (MOI 1) for 24 h. (**A**) A representative immunoblot of full-length TREM2 (TREM2) and C-terminal fragment (CTF) is shown. (**B**) Quantification of full-length TREM2 in uninfected (UI) microglia versus microglia infected with HSV1 (MOI 1) for 24 h. (**C**) sTREM2 levels in cell supernatants of UI versus HSV1-infected microglia 24 h post infection. (**D**) *TREM2* mRNA levels 24 h post infection with HSV1 at different MOI's as indicated. (**E**) *TREM2* mRNA levels 8 and 24 h post infection with HSV1 (MOI 1). (**F**) *TREM2* mRNA levels 24 h post infection with HSV1 MOI 1 with and without 50 µM Acyclovir. (**G**) *TREM2* mRNA 24 h after incubation with and without UV-inactivated HSV1 (MOI 1). (**H**) *TYROBP (DAP12)* mRNA levels

24 h post infection with HSV1 at different MOIs as indicated. (**I**) DAP12 protein levels 24 h post infection with HSV1 (MOI 1). A representative immunoblot is shown. (**J**) *IFNB*, *IL6*, *TNFA*, and *MX1* mRNA levels in UI microglia versus HSV1-infected microglia 24 h post infection (MOI 1). (**K**, **L**) cGAS was knocked down in hiPSC-derived microglia using siRNA. (**K**) Control and cGAS KD microglia were infected with HSV1 (MOI 3) for 5 h. Representative immunoblots for the cGAS-STING signaling pathway and cGAS are shown. (**L**) *IFNB*, *IL6*, *TNFA*, and *MX1* mRNA levels were analyzed in control versus cGAS KD microglia 24 h post infection with HSV1 (MOI 1). All figures represent at least 2-3 independent experiments; data are presented as mean ± SEM; *P* values were calculated by one-way ANOVA with Tukey's multiple comparisons test (F) and Mann-Whitney *U* test (B-E, G-H, J, L). ** P<0.001; *** P<0.0005; **** P<0.0001.

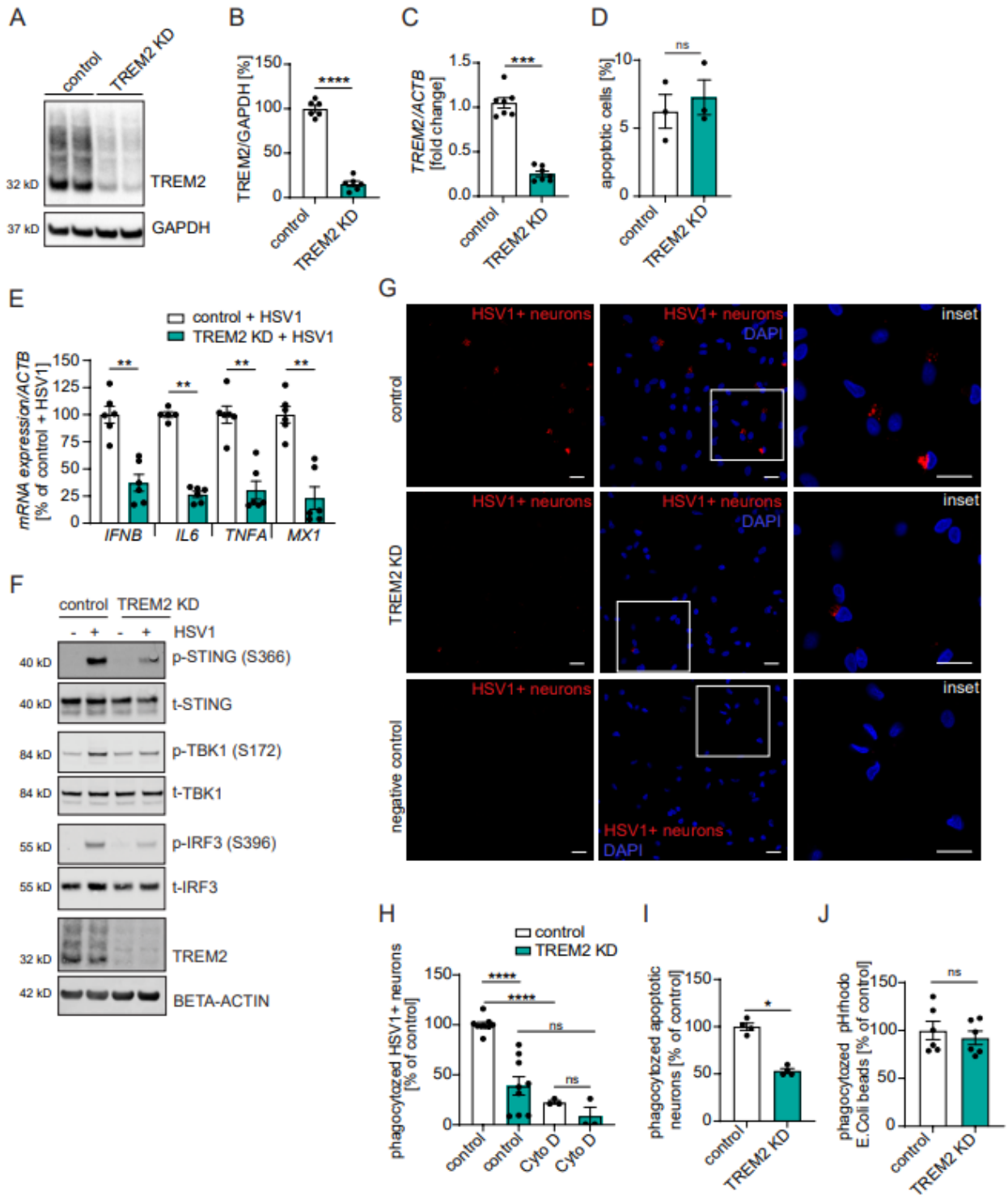

Fig. 3. **Depletion of TREM2 expression in microglia impairs innate immune responses to HSV1 *in vitro*.** (**A-G**) TREM2 was knocked down in hiPSC-derived microglia using siRNA. Cells

were used for experiments 4 days after transfection. (**A**) A representative immunoblot of full-length TREM2 (TREM2) of control and TREM2 KD microglia is shown. (**B**) Quantification of full-length TREM2 protein in control versus TREM2 KD microglia. (**C**) Quantification of *TREM2* mRNA in control and TREM2 KD microglia. (**D**) Apoptotic cells in control and TREM2 KD cultures were stained using an Annexin V antibody and quantified by flow cytometry. Quantification of apoptotic cells is shown. (**E**) *IFNB*, *IL6*, *TNFA*, and *MX1* mRNA levels were analyzed in control versus TREM2 KD microglia 24 h post infection with HSV1 (MOI 1). (**F**) Control and TREM2 KD microglia were infected with HSV1 (MOI 3) for 5 h. Representative immunoblots for the cGAS-STING signaling pathway and TREM2 are shown. (**G, H**) HiPSC-derived neurons were infected with HSV1 (MOI 1) for 24 h, stained with a fluorescent cell tracker and added to control and TREM2 KD microglia for 15 h. (**G**) Cells were fixed and imaged using a confocal microscope (red=HSV1-infected neurons; blue=DAPI). The negative control were untreated cells. Scale bar = 20 µm. (**H**) Cells that had phagocytosed HSV1-infected neurons were quantified by flow cytometry (PE channel). Cytochalasin D (Cyto D, 5 µM) was added to specifically block phagocytosis. (**I**) Control and TREM2 KD microglia were incubated with fluorescent cell tracker-stained apoptotic neurons for 15 h. Cells that had phagocytosed apoptotic neurons were quantified by flow cytometry (PE channel). (**J**) Control and TREM2 KD microglia were incubated with pHrodo-*E. coli* beads for 3 h. Phagocytosis of pHrodo-*E. coli* beads was quantified using a microplate reader. All figures represent 2-3 independent experiments; data are presented as mean ± SEM; *P* values were calculated by Mann-Whitney *U* test. * $P<0.05$; ** $P<0.001$; *** $P<0.0005$; **** $P<0.0001$.

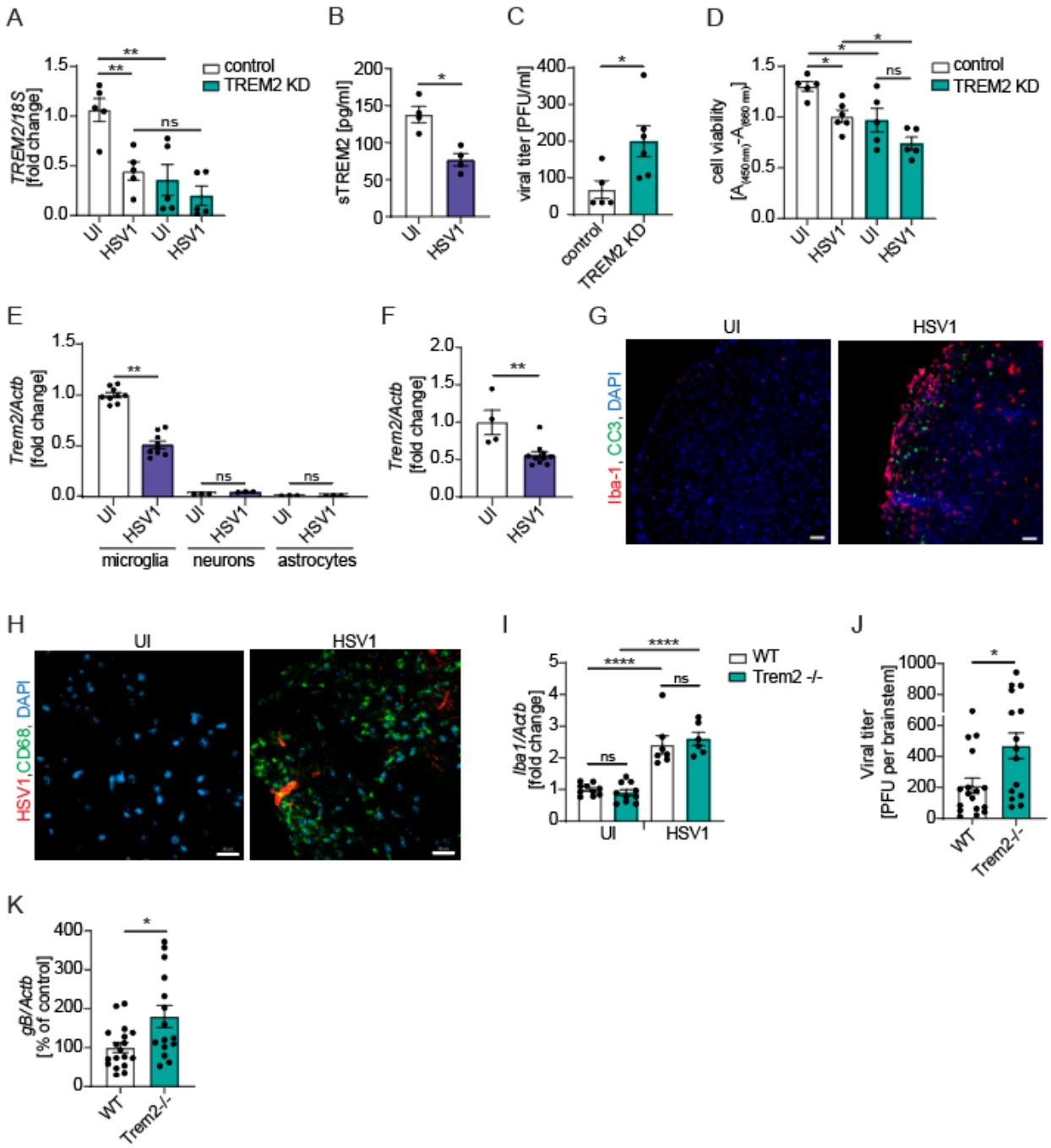

Fig. 4. **TREM2 is essential for control of HSV1 infection *in vitro* and *in vivo*.** (**A**) *TREM2* mRNA levels were analyzed 24 h post infection of hiPSC-derived co-cultures of microglia and neurons with HSV1 (MOI 1). (**B**) sTREM2 levels were measured in supernatants of co-cultures 24 h post infection with HSV1 (MOI 1) by ELISA. (**C**) Viral titers in co-culture supernatants 24 h post infection with HSV1 (MOI 1) were quantified by viral plaque assay. (**D**) Cell viability was measured in co-cultures 24 h post infection with HSV1 (MOI 1) using the CyQUANT XTT assay. Specific absorbance, which was calculated by using the formula: $A_{(450\ nm)}$-$A_{(660\ nm)}$, is shown and reflects cell viability. (**E**) *Trem2* mRNA levels were analyzed in primary murine microglia,

neurons, and astrocytes 6 h post infection with HSV1 (McKrea, MOI 3). (**F**) *Trem2* mRNA levels were analyzed in WT mouse brainstem 4 days post infection with HSV1 via the corneal route (2 × 10^6 PFU/cornea). (**G**, **H**) WT mice were infected with HSV1 (2 × 10^6 PFU/cornea), brainstems were isolated and stained 5 days post infection. Representative images are shown. (**G**) Tissue sections were stained for Iba-1 (red) and CC3 (green). Scale bar = 50 µm, (**H**) Tissue sections were stained for HSV1 (red) and CD68 (green). Scale bar = 20 µm. (**I**, **K**) *Iba1* and *gB* mRNA levels were quantified in brainstem of WT and Trem2 -/- mice 4 days post infection with HSV1 via the corneal route (2 × 10^6 PFU/cornea). (**J**) Viral titers of isolated brainstems 4 days post infection with HSV1 via the corneal route (2 × 10^6 PFU/cornea) were quantified by plaque assay. All figures represent 2-3 independent experiments; n = 15-18 per group of mice; data are presented as mean ± SEM; P values were calculated by one-way ANOVA with Tukey's multiple comparisons test (A, D, K) and Mann-Whitney test U (B, C, E, f, I, J). * P<0.05; ** P<0.001; **** P<0.0001.

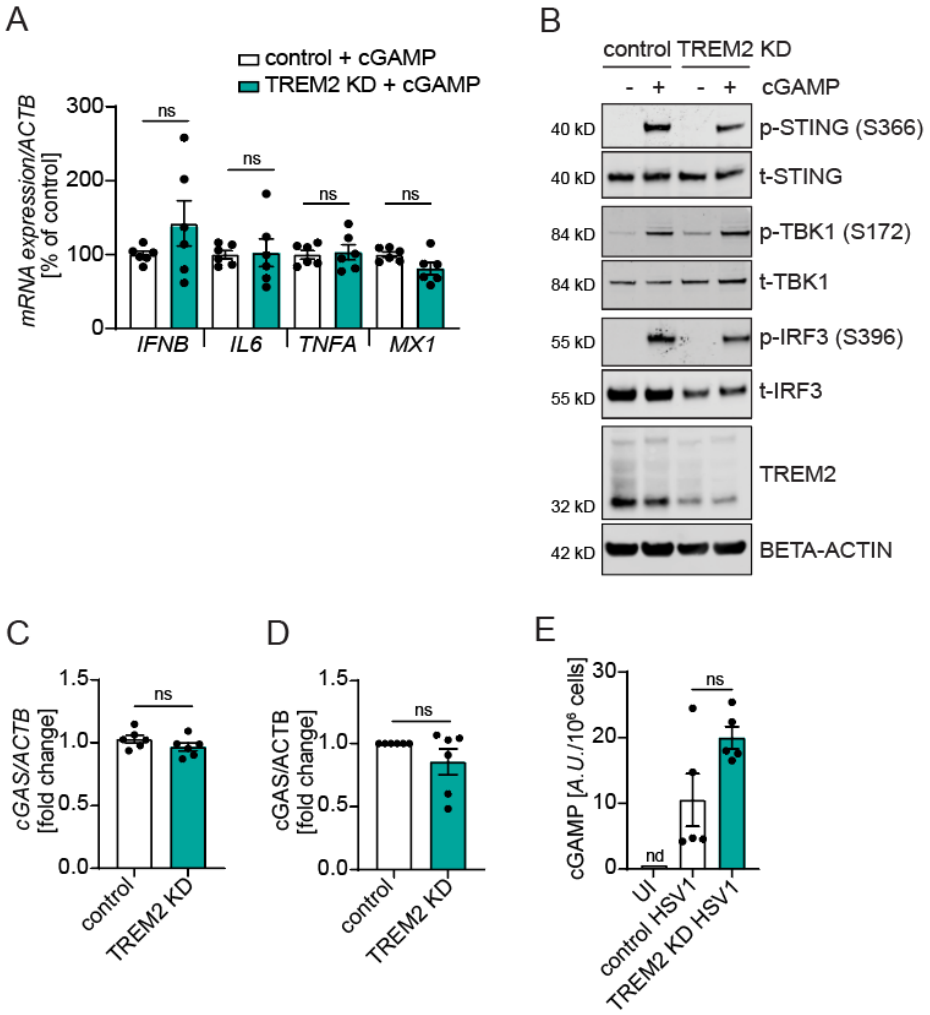

Fig. 5. **The antiviral program is not impaired in response to cGAMP in TREM2 depleted hiPSC-derived microglia.** (**A, B**) Control and TREM2 KD microglia were stimulated with 100 µM cGAMP for 5 h. (**A**) *IFNB*, *IL6*, *TNFA*, and *MX1* mRNA levels are shown. (**B**) Representative immunoblots of the cGAS-STING axis and TREM2 are shown. (**C**) *cGAS* mRNA levels are shown in control and TREM2 KD microglia. (**D**) Quantification of cGAS protein levels in control and TREM2 KD microglia is shown. (**E**) Quantification of cGAMP levels in HSV1-infected control versus TREM2 KD microglia 24 h post-infection. cGAMP was not detectable (nd) in UI cells, instead the detection limit is shown. *A.U.* arbitrary units. All figures represent 2-3 independent experiments; data are presented as mean ± SEM; *P* values were calculated by Mann-Whitney *U* test.

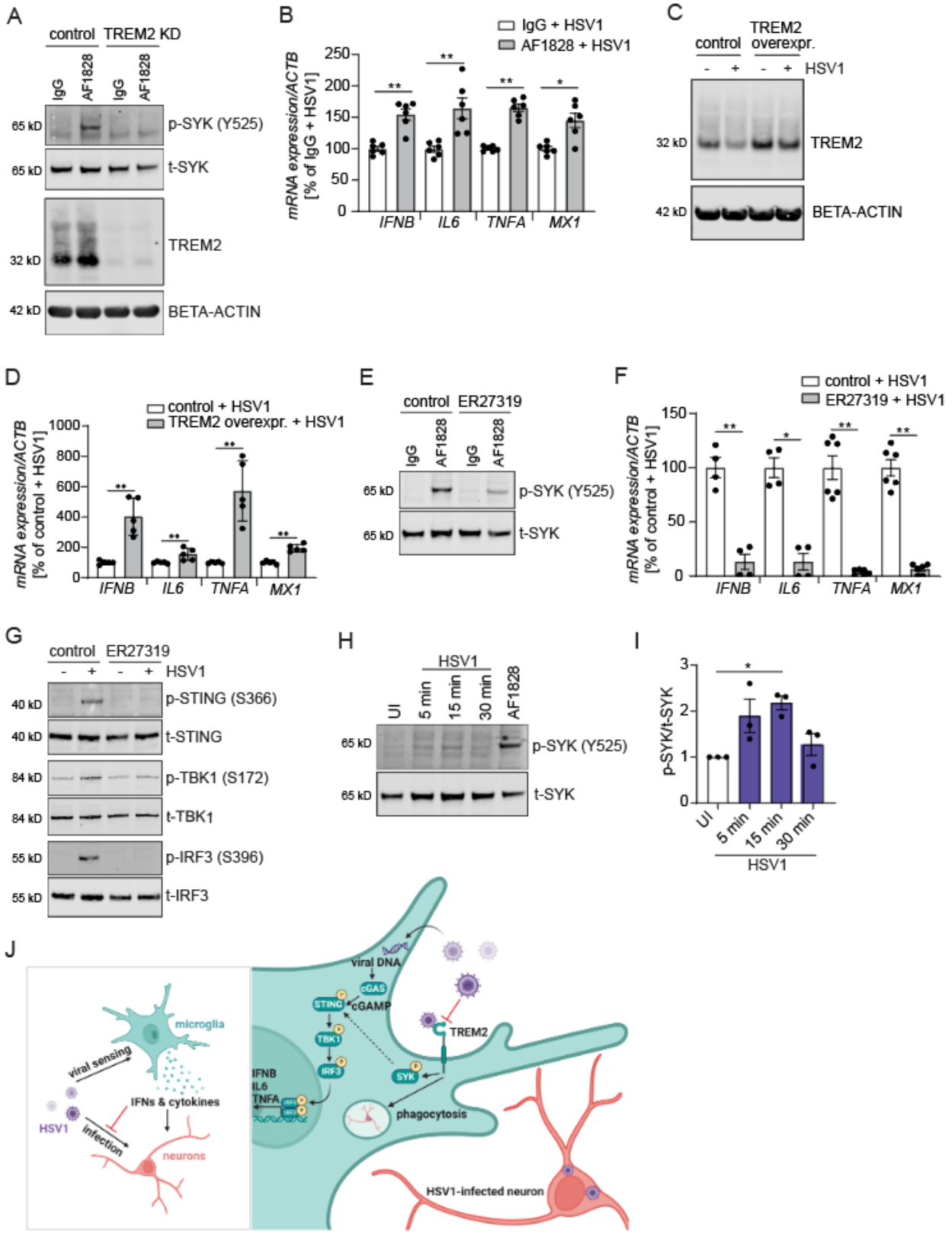
A
control
TREM2 KD
IgG
AF1828
IgG
AF1828
65 kD
p-SYK (Y525)
65 kD
t-SYK
32 kD
TREM2
42 kD
BETA-ACTIN
B
IgG + HSV1
AF1828 + HSV1
mRNA expression/ACTB [% of IgG + HSV1]
IFNB
IL6
TNFA
MX1
C
control
TREM2 overexpr.
HSV1
32 kD
TREM2
42 kD
BETA-ACTIN
D
control + HSV1
TREM2 overexpr. + HSV1
mRNA expression/ACTB [% of control + HSV1]
IFNB
IL6
TNFA
MX1
E
control
ER27319
IgG
AF1828
IgG
AF1828
65 kD
p-SYK (Y525)
65 kD
t-SYK
F
control + HSV1
ER27319 + HSV1
mRNA expression/ACTB [% of control + HSV1]
IFNB
IL6
TNFA
MX1
G
control
ER27319
HSV1
40 kD
p-STING (S366)
40 kD
t-STING
84 kD
p-TBK1 (S172)
84 kD
t-TBK1
55 kD
p-IRF3 (S396)
55 kD
t-IRF3
H
HSV1
UI
5 min
15 min
30 min
AF1828
65 kD
p-SYK (Y525)
65 kD
t-SYK
I
p-SYK/t-SYK
UI
5 min
15 min
30 min
HSV1
J
microglia
viral sensing
IFNs & cytokines
HSV1
infection
neurons
viral DNA
cGAS
STING
cGAMP
TBK1
IRF3
IFNB
IL6
TNFA
SYK
TREM2
phagocytosis
HSV1-infected neuron

Fig. 6. **Modulation of TREM2 activity via SYK modulates the innate immune response to HSV1 infection in hiPSC-derived microglia.** (**A**) Control and TREM2 KD microglia were incubated with 0.8 µg/ml control IgG or the TREM2-activating antibody AF1828 for 15 min. Representative immunoblots of p-SYK and TREM2 are shown. (**B**) *IFNB*, *IL6*, *TNFA*, and *MX1* mRNA levels were analyzed in microglia after infection with HSV1 (MOI 1) in combination with control IgG or AF1828 for 8 h. (**C**) Control and TREM2-overexpressing microglia were infected with HSV1 (MOI 1) for 24 h. A representative immunoblot of TREM2 is shown. (**D**) *IFNB*, *IL6*, *TNFA*, and *MX1* mRNA levels were analyzed in control and TREM2-overexpressing microglia after infection with HSV1 (MOI 1) for 24h. (**E**) Microglia were incubated with 0.8 µg/ml control IgG or AF1828 and with vehicle control or 5 µM ER27319 (SYK inhibitor) for 10 min. A representative immunoblot of p-SYK is shown. (**F**) Microglia were infected with HSV1 (MOI 1) with vehicle control or 5 µM ER27319 for 8 h. *IFNB*, *IL6*, *TNFA*, and *MX1* mRNA levels are shown. (**G**) Microglia were incubated with vehicle control or 5 µM ER27319 and were infected with HSV1 (MOI 3) for 5 h. Representative immunoblots for the cGAS-STING signaling pathway are shown. (**H, I**) Microglia were infected with HSV1 (MOI 5) for the indicated time points or stimulated with 0.8 µg/ml AF1828 for 30 min. (**H**) A representative immunoblot is shown. (**I**) Quantification of p-SYK/t-SYK from three independent experiments is shown. (**J**) Illustration of the roles of microglial TREM2 during viral CNS infection. All figures represent 2-3 independent experiments; data are presented as mean ± SEM; *P* values were calculated by Mann-Whitney *U* test (B, D, F) and one-way ANOVA with Tukey's multiple comparisons test (I). * $P<0.05$; ** $P<0.001$.

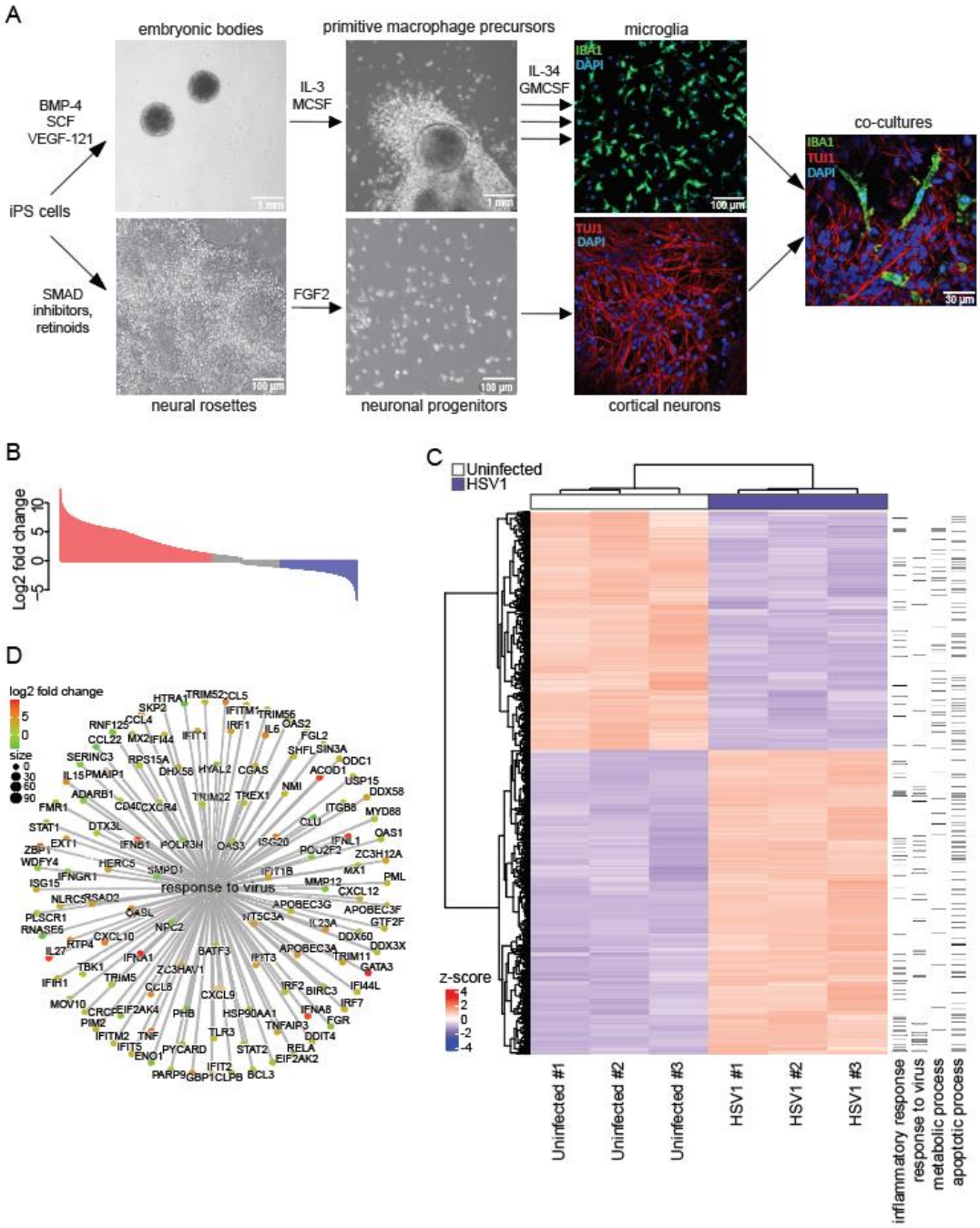

Fig. S1. Stem cell differentiation workflow and RNA-seq data analysis of hiPSC-derived microglia. (**A**) Illustration of the differentiation workflow from hiPSCs towards microglia and cortical neurons is shown. Cells were stained for markers for microglia (IBA1, green), cortical neurons (TUJ1, red), and nuclei (DAPI, blue). Multiple arrows indicate continuous harvest of microglia. (**B**) Waterfall plot for RNA-seq of HSV1-infected microglia relative to uninfected microglia. (**C**) Hierarchical clustering of genes differentially expressed in uninfected versus HSV1-infected microglia. Biological function annotated with the regulated genes is shown on the right. (**D**) Differentially regulated genes in the gene ontology category "response to virus" in HSV-infected microglia.

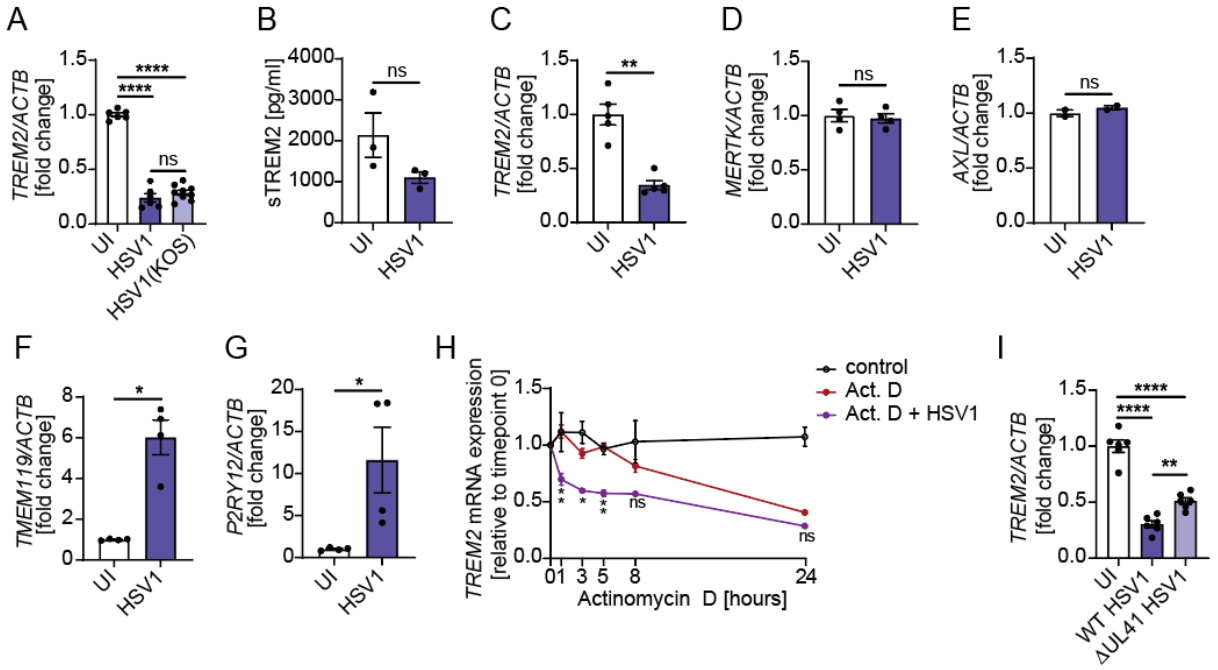

Fig. S2. **HSV1 downregulates microglial TREM2 expression independent of the viral strain and iPSC line used.** (**A**) *TREM2* mRNA levels were analyzed 24 h post infection of hiPSC-derived microglia with the clinical HSV1 strain (MOI 1) and the KOS strain (MOI 1). (**B**, **C**) Microglia differentiated from a separate iPSC line (ChiPSC22). (**B**) sTREM2 levels were analyzed 24 h post infection with HSV1 (MOI 1) by ELISA. (**C**) *TREM2* mRNA levels were analyzed 24 h post infection with HSV1 (MOI 1). (**D**-**G**) Examples of genes which mRNA levels were unchanged (*MERTK* and *AXL*) or upregulated (*TMEM119* and *P2RY12*) in microglia 24 h post infection with HSV1 (MOI 1). (**H**) Microglia were incubated with vehicle control or 5 µg/ml Actinomycin D for the indicated time points in presence and absence of HSV1 infection (MOI3). *TREM2* mRNA decay was quantified. (**I**) *TREM2* mRNA levels were analyzed 24 h post infection with wildtype (WT) HSV1 and a UL41 mutant strain (ΔUL41). All figures represent 2-3 independent experiments; data are presented as mean ± SEM; *P* values were calculated by one-way ANOVA with Tukey's multiple comparisons test (A and H) and Mann-Whitney *U* test (B-G). * P<0.05; ** P<0.001; **** P<0.0001.

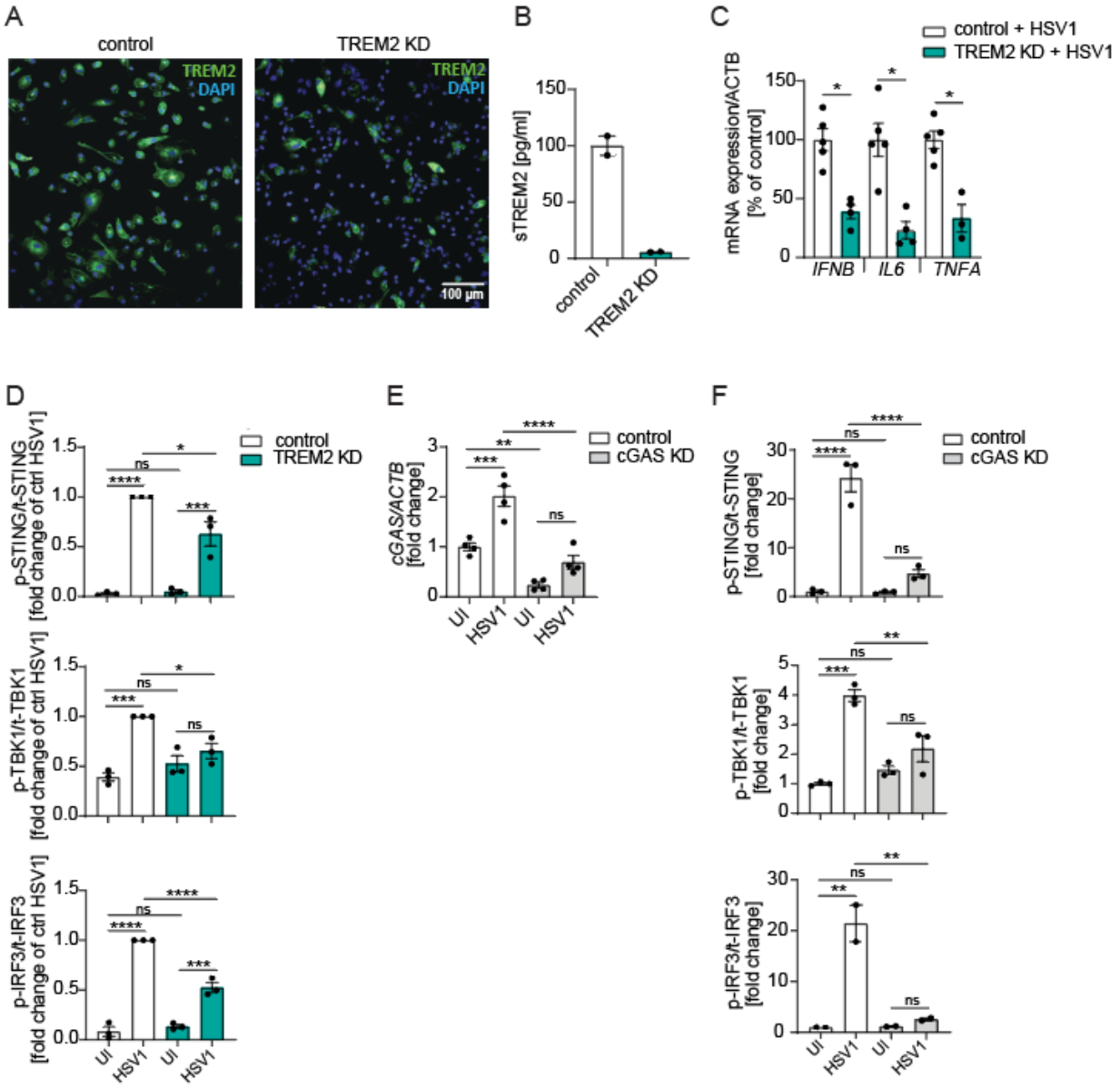

Fig. S3. **Characterization of TREM2 KD hiPSC-derived microglia.** (**A**) Control and TREM2 KD microglia were stained for TREM2 (green) and DAPI (blue) and imaged using a confocal microscope. (**B**) sTREM2 levels were measured in in cell supernatants by ELISA. All figures represent 2 independent experiments; data are presented as mean ± SEM. (**C**) Microglia differentiated from a separate iPSC line (ChiPSC22). *IFNB*, *IL6*, and *TNFA* mRNA levels were analyzed 24 h post infection with HSV1 (MOI 3). (**D**) Quantifications of Fig. 3F (**E**) cGAS was knocked down in microglia using siRNA. Cells were used for experiments 4 days after transfection. Control and cGAS KD microglia were infected with HSV1 (MOI 3) for 24 h. *cGAS* mRNA levels were quantified. (**F**) Quantifications of Fig. 2K. All figures represent 2-3 independent experiments; data are presented as mean ± SEM; *P* values were calculated by Mann-Whitney *U* test (B,C) and one-way ANOVA with Tukey's multiple comparisons test (D-F). * P<0.05; ** P<0.001; *** P<0.0005; **** P<0.0001.

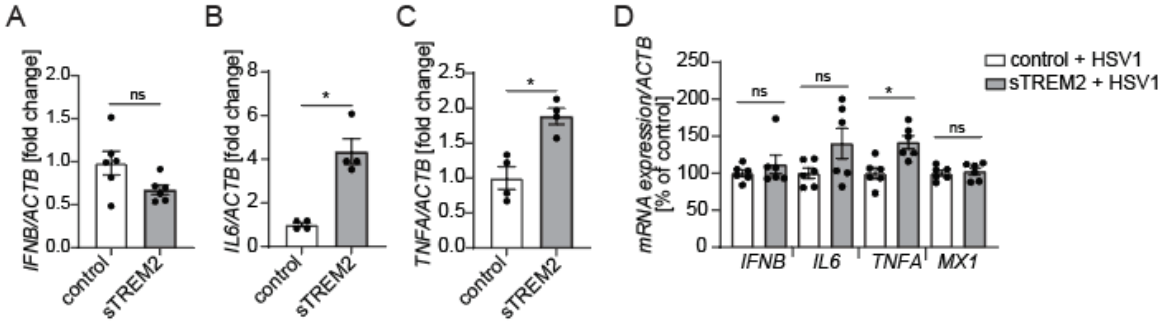

Fig. S4. **sTREM2 activates inflammatory responses but not antiviral defense.** (**A**-**C**) HiPSC-derived microglia were incubated with 3 µg/ml sTREM2 for 24 h. *IFNB*, *IL6*, and *TNFA* mRNA levels are shown. (**D**) *IFNB*, *IL6*, *TNFA*, and *MX1* mRNA levels were analyzed in microglia after infection with HSV1 (MOI 1) with and without sTREM2 for 8 h. All figures represent 2-3 independent experiments; data are presented as mean ± SEM; *P* values were calculated by Mann-Whitney test. * P<0.05.

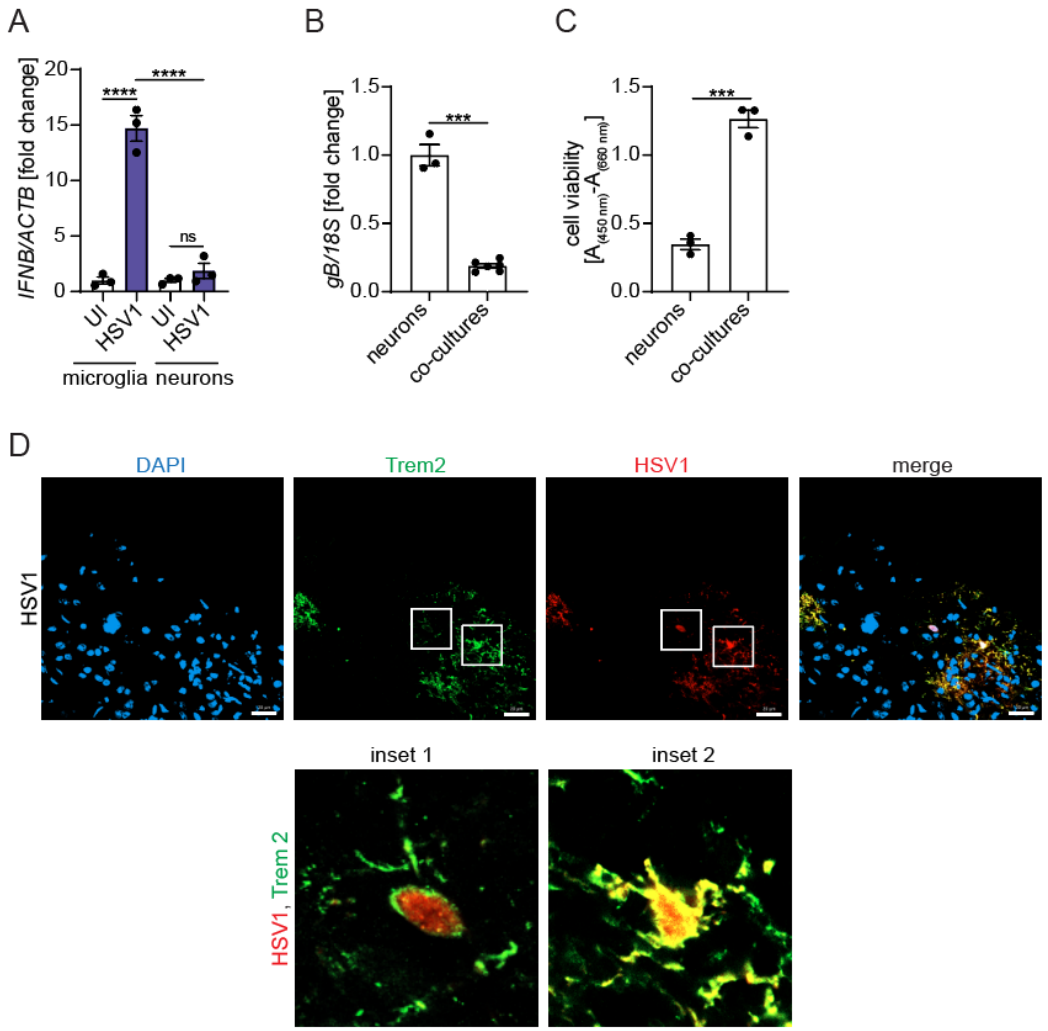

Fig. S5. **Microglia are the main source of IFNB and decrease viral replication in co-cultures compared with neurons alone.** (**A**) *IFNB* mRNA levels were analyzed in hiPSC-derived microglia and neurons 24 h after infection with HSV1 (MOI 1). (**B**, **C**) HiPSC-derived neurons and co-cultures of microglia and neurons were analyzed 24 h after infection with HSV1 (MOI 1). (**B**) *gB* mRNA levels are shown. (**C**) Cell viability is shown. (**D**) WT mice were infected with HSV1 (2×10^6 PFU/cornea), brainstems were isolated and stained 5 days post infection. Tissue sections were stained for HSV1 (red) and Trem2 (green). Representative images are shown. Scale bar = 20 µm. Two insets are magnified without DAPI. All figures represent 1-2 independent experiments; data are presented as mean ± SEM; *P* values were calculated by two-way ANOVA with Tukey's multiple comparisons test (A) and two-tailed Student's *t*-test (B, C). *** P<0.0005; **** P<0.0001.

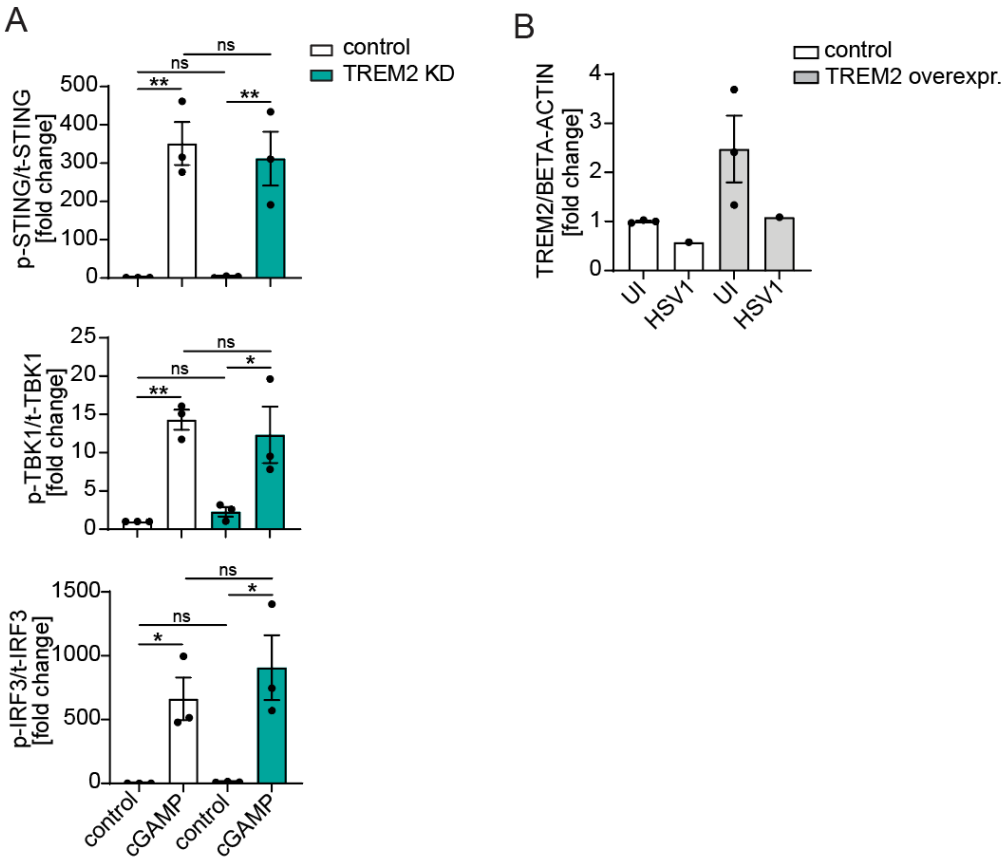

Fig. S6. Quantification of cGAS/STING signaling in cGAMP-stimulated microglia. (**A**) Quantifications of Fig. 5B are shown. (B) Quantification of Fig. 6C. (A) represents three independent experiments; (B) represents one experiment. Data are presented as mean ± SEM; *P* values were calculated by one-way ANOVA with Tukey's multiple comparisons test. * P<0.05; ** P<0.001.